# Magnetoelectric Magnetometers

**Mirza I. Bichurin, Vladimir M. Petrov, Roman V. Petrov
and Alexander S. Tatarenko**

**Abstract** Key features of magnetoelectric (ME) sensors for measuring the magnetic field, electric current and microwave power are discussed. ME sensors are shown to have advantages over semiconductor ones in the sensitivity, low price and radiation resistance. To predict the feasibility of a composite for sensor application, we propose the nomograph method based on given parameters of the composite components. The sensor sensitivity depends on the construction and the materials parameters of the ME composite and bias magnetic field. ME laminates offer opportunities for low frequency ($10^{-2}$–$10^3$ Hz) detection of low magnetic fields ($10^{-12}$ Tesla or below) at room temperature in a passive mode of operation. Any other magnetic sensor does not reveal such combinations of characteristics. Current sensing based on ME effect is a good choice for many applications due to galvanic isolation between the current and measuring circuit. For increasing the sensor sensitivity one needs to use the ME composite based on materials with high magnetostriction and strong piezoelectric coupling. Microwave power sensors based on composite materials have a wide frequency range up to hundreds of gigahertz, stable to significant levels of radiation, and a temperature range from 0 K to the Curie temperature. In the microwave region, it is possible to use selective properties of ME materials, that enables one to create a frequency-selective power sensor with fine-tuning.

## 1 Introduction

In this chapter under the magnetoelectric (ME) sensors, we understand the devices recording the magnetic field, current in conductor, microwave power and so on, at that the ME composites are the working material of these devices. In the ME composites ferromagnetism and ferroelectricity occur simultaneously and coupling between the two is enabled and connected with the ME effect. The ME effect is defined as the dielectric polarization response of a material to an applied magnetic

M.I. Bichurin (✉) · V.M. Petrov · R.V. Petrov · A.S. Tatarenko
Novgorod State University, Veliky Novgorod, Russia
e-mail: mirza.bichurin@novsu.ru

field, or an induced magnetization change upon application of an external electric field [1, 2]. The Tellegen's gyrator was the first offered ME device [3], which was realized later based on layered structure of Terfenol—PZT [4]. The main interest of researchers referring to design of magnetic field sensors was connected with obtained high value of ME effect. This result showed the opportunity of design based on ME composites of high sensitivity magnetic field sensors working at room temperature [5]. The latest obtained results in the area of magnetic sensor design presented in the review of Viehland et al. [6].

The chapter is organized as follows:

In Sec. 2, we briefly discuss the ME effect in composites; define ME voltage coefficients (MVC) at the low-frequency, electromechanical (EMR) and ferromagnetic resonance (FMR) ranges and make an example of calculation of MVC by nomographs. In Sec. 3, the results of the investigations of the ME magnetic field sensors including the physical and noise models; fabrication and electronics with applications examples are reported. In Sec. 4, we present the ME current sensors with physical model and fabrication and electronics. In Sec.5, the ME microwave power sensors are considered. The equivalent circuit and fabrication of such sensors are described.

## 2  Magnetoelectric Composites

In ME composites the induced polarization P is related to the magnetic field H by the expression, $P = \alpha H$, where a is the second rank ME-susceptibility tensor. The (static) effect was first observed in antiferromagnetic $Cr_2O_3$. But most single phase compounds show only weak ME interactions and only at low temperatures [7]. However, composites of piezomagnetic/piezoelectric phases are also magnetoelectric [8, 9]. When said composites are subjected to a bias magnetic field H, a magnetostriction induced strain is coupled to the ferroelectric phase that results in an induced electric field E via piezoelectricity. The ME susceptibility, $\alpha = \delta P/\delta H$, is the product of the piezomagnetic deformation $\delta l/\delta H$ and the piezoelectric charge generation $\delta P/\delta l$ [10]. Here we are primarily interested in the dynamic ME effect. For an ac magnetic field $\delta H$ applied to a biased laminate composite, one measures the induced voltage $\delta V$. The ME voltage coefficient $\alpha_E = \delta E/\delta H = \delta V/t \; \delta H$(or $a = \varepsilon_o \varepsilon_r \; \alpha_E$), where t is the composite thickness and $\varepsilon_r$ is the relative permittivity [10]. The ME effect was first observed in single crystals [11] of single phase materials a little more 50 years ago, and subsequently in polycrystalline single phase materials. The largest value of $\alpha_{ME}$ for a single phase material is that for $Cr_2O_3$ crystals [11], where $\alpha_{ME} = 20$ mV/cm Oe. In last few years, strong magneto-elastic and elasto-electric coupling has been achieved through optimization of material properties and proper design of transducer structures. Lead zirconate titanate (PZT)-ferrite, PZT-Terfenol-D and PZT-Metglas are the most studied composites to-date [12–14]. One of largest ME voltage coefficient of 500 V $cm^{-1}$ $Oe^{-1}$ was reported recently for a high permeability magnetostrictive

piezofiber laminate [14]. These developments have led to ME structures that provide high sensitivity over a varying range of frequency and dc bias fields enabling the possibility of practical applications [15, 16].

In order to obtain high ME couplings, a layered structure must be insulating, in order that it can be poled to align the electric dipole moments. The poling procedure involved heating the sample to 420 K, and re-cooling to 300 K under an electric field of E = 20–50 kV/cm. The samples are then placed between the pole pieces of an electromagnet (0–18 kOe) used for applying a magnetic bias field H. The required ac magnetic field $\delta H = 1$ Oe at 10 Hz–100 kHz applied parallel to H is generated with a pair of Helmholtz coils. The ac electric field $\delta E$ perpendicular to the sample plane is estimated from the measured voltage $\delta V$. The ME coefficient $a_E$ is measured for three conditions: (1) transverse or $\alpha_{E,31}$ for H and $\delta H$ parallel to each other and to the disk plane (1,2) and perpendicular to $\delta E$ (direction-3), (2) longitudinal or $\alpha_{E,33}$ for all the three fields parallel to each other and perpendicular to sample plane and (3) in-plane $\alpha_{E,11}$ for all the three fields parallel to each other and parallel to sample plane. An ME phenomenon of fundamental and technological interests is an enhancement in the coupling, when the electrical or magnetic sub-system undergoes resonance: i.e., electromechanical resonance (EMR) for PZT and ferromagnetic resonance (FMR) for the ferrite. As the dynamic magnetostriction is responsible for the electromagnetic coupling, EMR leads to significant increasing in the ME voltage coefficients. In case of resonance ME effects at FMR an electric field E produces a mechanical deformation in the piezoelectric phase, resulting in a shift in the resonance field for the ferromagnet. Besides, the peak ME voltage coefficient occurs at the merging point of acoustic resonance and FMR frequencies, i.e., at the magnetoacoustic resonance [10]. Then we discuss the estimations of ME effects in the different frequency ranges.

## 2.1 Low-Frequency ME Coupling

We consider more often used in practice the transverse fields' orientation that corresponds to $E$ and $\delta E$ being applied along the $X_3$ direction, and $H$ and $\delta H$ along the $X_1$ direction (in the sample plane). The expression for the transverse ME voltage coefficient is [17, 18]

$$\alpha_{E,31} = \frac{E_3}{H_1} = \frac{-V(1-V)(^m q_{11} + {}^m q_{21})^p d_{31}}{{}^p \varepsilon_{33}(^m s_{12} + {}^m s_{11})v + {}^p \varepsilon_{33}(^p s_{11} + {}^p s_{12})(1-V) - 2^p d_{31}^2 (1-V)} \quad (1)$$

For symmetric trilayer structures, using the 1-D approximations, the expression for transverse ME voltage coefficient takes on the form:

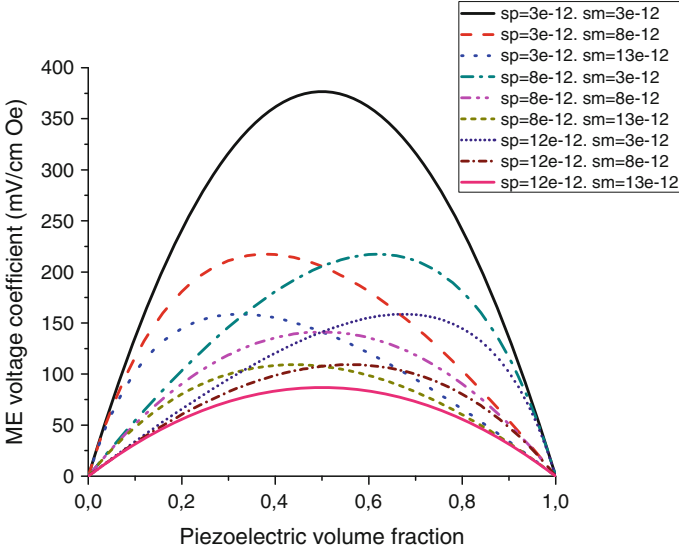$$\alpha_{E,31} = \frac{V(1-V)x}{\varepsilon_0 [^m s_{11} V + {}^p s_{11}(1-V)]} \quad (2)$$

**Fig. 1** Piezoelectric volume fraction dependence of transverse ME voltage coefficient for symmetric layered structure of magnetostrictive and piezoelectric components with different compliencecs

where $x = ({}^{m}q_{11} + {}^{m}q_{12})\frac{{}^{p}d_{31}}{{}^{p}\varepsilon_{33}/\varepsilon_0}$, $s_p = {}^{p}s_{11}(1 - {}^{p}v)$, $s_m = {}^{m}s_{11}(1 - {}^{m}v)$, ${}^{p}s_{11}$, ${}^{m}s_{11}$, ${}^{p}d_{31}$ and ${}^{m}q_{11}$ are compliance, and piezoelectric and piezomagnetic coupling coefficients for piezoelectric and piezomagnetic layers, respectively, ${}^{p}\varepsilon_{33}$ is the permittivity of piezoelectric layer. In Eq. 2, the electromechanical coupling factor is assumed to satisfy the condition: ${}^{p}K_{31}^{2} = {}^{p}d_{31}^{2}/{}^{p}s_{11}{}^{p}\varepsilon_{33} \ll 1$.

For convenience we suggest using the nomograph method that facilitates the efficient estimates of ME voltage coefficients from given parameters of composite components (Figs. 1 and 2).

For the bilayer structure, the ME voltage coefficient should be calculated taking into account the flexural deformations. On the foregoing assumptions, our model enables deriving the explicit expression for ME voltage coefficient:

$$\frac{\delta E_3}{\delta H_1} = \frac{[1{}^{p}s_{11} + {}^{m}s_{11}r^3]{}^{m}q_{11}{}^{p}d_{31}/{}^{p}\varepsilon_{33}}{{}^{p}s_{11}[2r{}^{m}s_{11}(2 + 3r + 2r^2) + {}^{p}s_{11}] + {}^{m}s_{11}^{2}r^4} \tag{3}$$

Equation 3 is written in a simplified form under assumption ${}^{p}K_{31}^{2} \ll 1$ similarly to deriving Eq. 2 (Figs. 3 and 4).

## 2.2 ME Coupling at Bending Mode

Next we consider ME coupling under small-amplitude flexural oscillations of a bilayer rigidly clamped at one end. The bilayer deflection should obey the equations
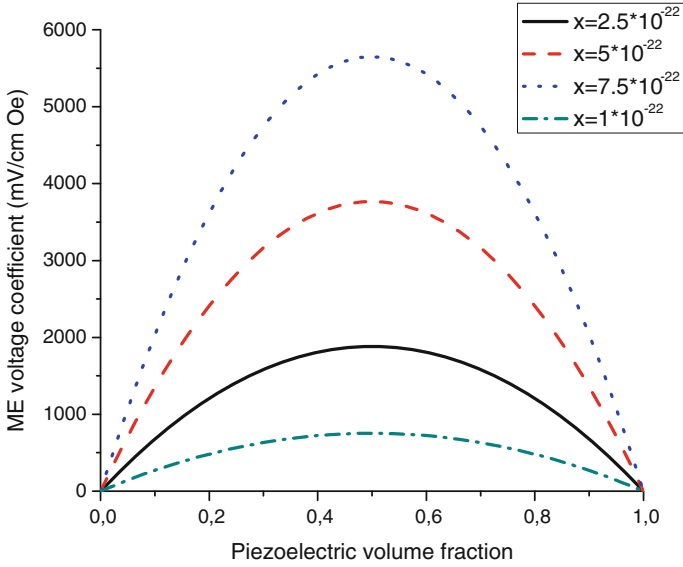
**Fig. 2** Piezoelectric volume fraction dependence of transverse ME voltage coefficient for symmetric layered structure of magnetostrictive and piezoelectric components at different × values
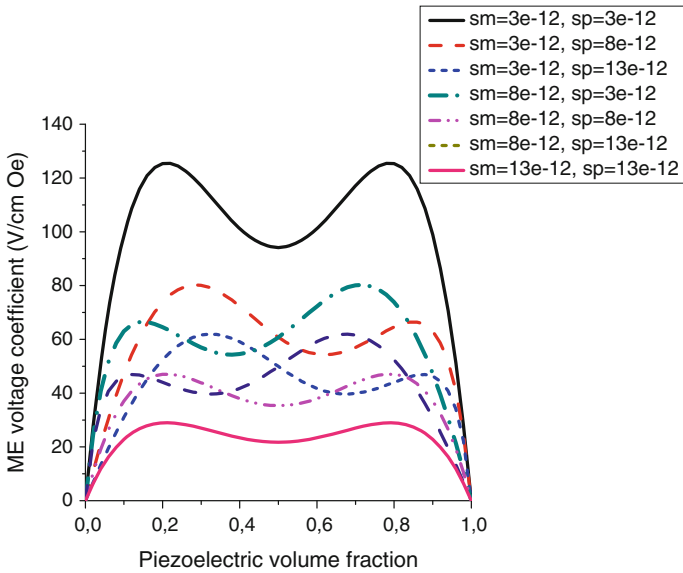


**Fig. 3** Piezoelectric volume fraction dependence of transverse ME voltage coefficient for bilayer of magnetostrictive and piezoelectric components with different compliencecs
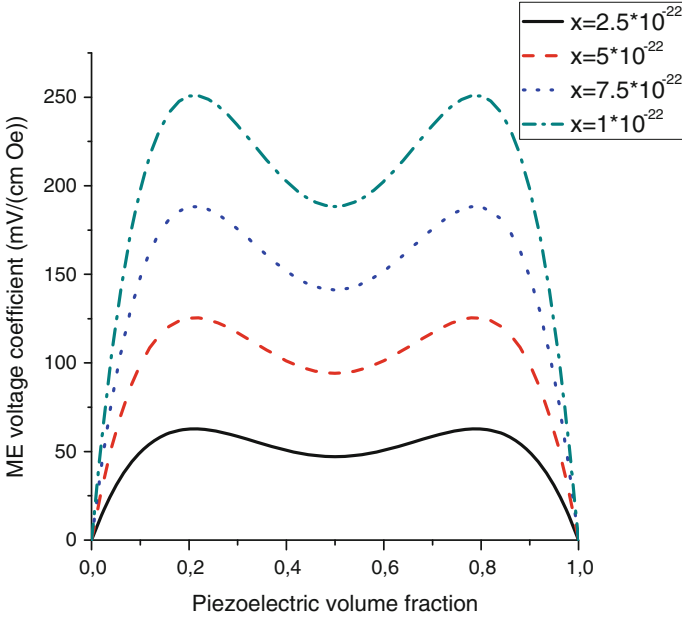
**Fig. 4** Piezoelectric volume fraction dependence of transverse ME voltage coefficient for bilayer of magnetostrictive and piezoelectric components at different × values in SI units with $x = {}^{m}q_{11}{}^{p}d_{31}\varepsilon_0/{}^{p}\varepsilon_{33}$

of bending motion provided in our models in Ref. [18]. To solve these equations, we used the boundary conditions that the bilayer deflection and its derivative vanish at clamped end of the bilayer and rotational moment and transverse force vanish at free end. Under assumption ${}^{P}K_{31}^{2} \ll 1$ and ${}^{m}K_{11}^{2} \ll 1$ (${}^{m}K_{11}^{2} = {}^{m}q_{11}^{2}/({}^{m}s_{11}{}^{m}\mu_{11})$ with ${}^{m}\mu_{11}$ denoting the absolute permeability of magnetic layer), the resonance condition is $\cosh(kL) \cdot \cos(kL) = -1$ where k is wave number.

The ME voltage coefficient at bending mode frequency can be estimated as

$$\alpha_{E31} = \frac{{}^{m}Y^{H} \cdot {}^{m}t \cdot {}^{P}d_{31} \cdot {}^{P}Y^{E} \cdot {}^{m}q_{11}(2 \cdot z_0 + {}^{m}t) \cdot (2 \cdot z_0 - {}^{P}t)}{2D\Delta \cdot {}^{P}\varepsilon_{33}}(r_4 r_1 + r_2 r_3) \qquad (4)$$

where $k^4 = \frac{\omega^2 \rho t}{D}$, $D$, $\rho$, $t$, and $L$ are cylindrical stiffness, density, total thickness, and length of sample, $\Delta = (r_1^2 + 2r_1 r_3 + r_3^2 - r_2^2 + r_4^2)kL$, $r_1 = \cosh(kL)$, $r_2 = \sinh(kL)$, $r_3 = \cos(kL)$, $r_4 = \sin(kL)$. Equation (8) shows that the bending resonance frequency is determined by equation $\Delta = 0$ and depends mainly on elastic compliances and volume fractions of initial components, and ratio $\frac{L}{\sqrt{t}}$. The peak ME voltage coefficient is dictated by Q value, piezoelectric and piezomagnetic coupling coefficients, elastic compliances and volume fractions of initial components (Figs. 5, 6, 7 and 8).
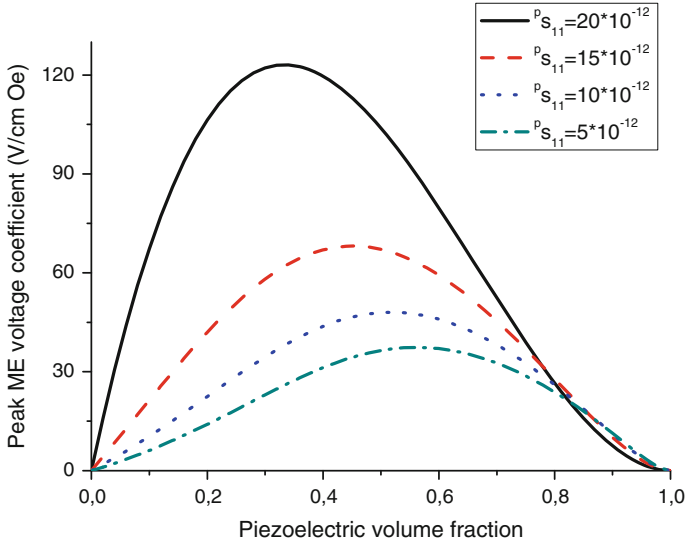
**Fig. 5** Piezoelectric volume fraction dependence of peak ME voltage coefficient at bending mode of magnetostrictive-piezoelectric bilayer for $^{m}s_{11} = 5 \times 10^{-12}$ m²/N and $^{p}s_{11} = 5 \times 10^{-12}$ m²/N (1), $^{p}s_{11} = 10 \times 10^{-12}$ m²/N (2), $^{p}s_{11} = 15 \times 10^{-12}$ m²/N (3), and $^{p}s_{11} = 20 \times 10^{-12}$ m²/N (4)
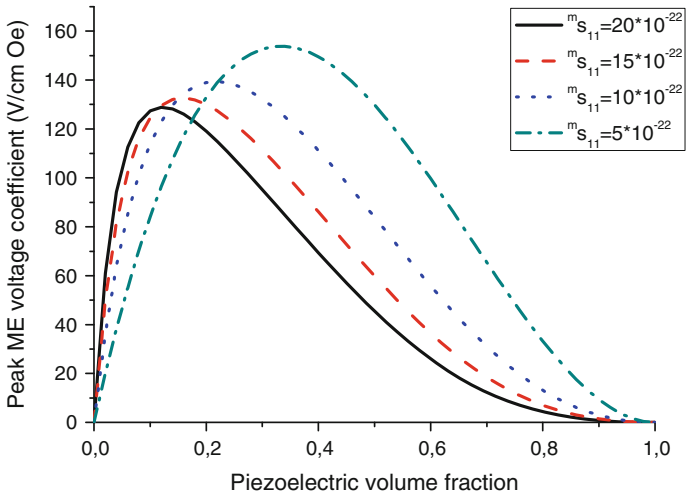


**Fig. 6** Piezoelectric volume fraction dependence of peak ME voltage coefficient at bending mode of magnetostrictive-piezoelectric bilayer for $^{p}s_{11} = 5 \times 10^{-12}$ m²/N and $^{m}s_{11} = 5 \times 10^{-12}$ m²/N (1), $^{m}s_{11} = 10 \times 10^{-12}$ m²/N (2), $^{m}s_{11} = 15 \times 10^{-12}$ m²/N (3), and $^{m}s_{11} = 20 \times 10^{-12}$ m²/N (4)

**Fig. 7** Piezoelectric volume fraction dependence of bending resonance frequency of magnetostrictive-piezoelectric bilayer for $^m s_{11} = 5 \times 10^{-12}$ m²/N and $^p s_{11} = 5 \times 10^{-12}$ m²/N (1), $^p s_{11} = 10 \times 10^{-12}$ m²/N (2), $^p s_{11} = 15 \times 10^{-12}$ m²/N (3), and $^p s_{11} = 20 \times 10^{-12}$ m²/N (4). Curves (a), (b), and (c) correspond to $Lt^{-\frac{1}{2}} = 0.2$ m^½, 1 m^½, and 2 m^½, correspondingly
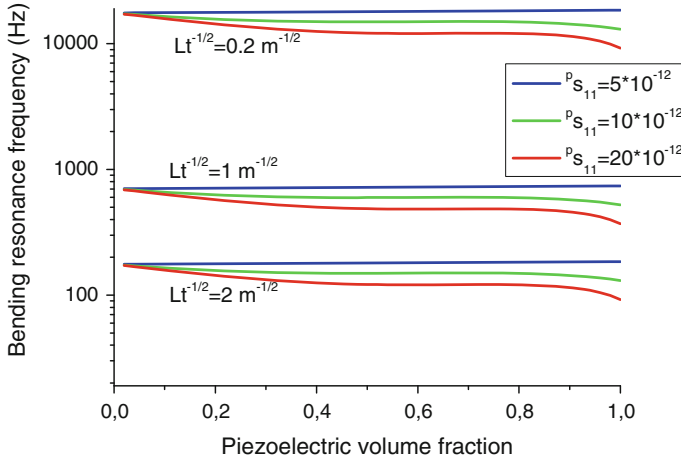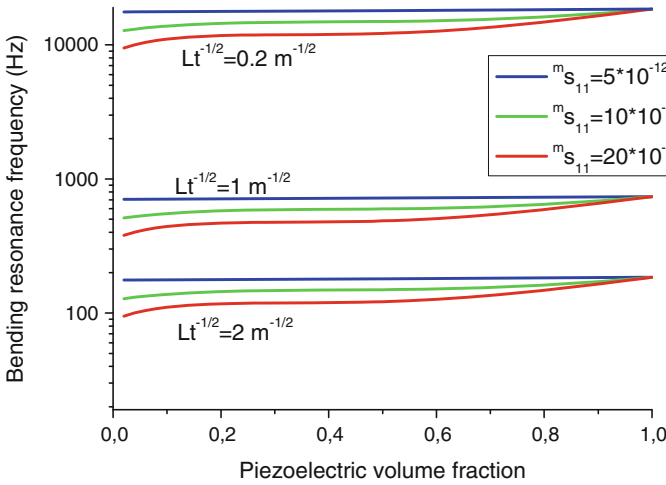


**Fig. 8** Piezoelectric volume fraction dependence of bending resonance frequency of magnetostrictive-piezoelectric bilayer for $^p s_{11} = 5 \times 10^{-12}$ m²/N and $^m s_{11} = 5 \times 10^{-12}$ m²/N (1), $^m s_{11} = 10 \times 10^{-12}$ m²/N (2), $^m s_{11} = 15 \times 10^{-12}$ m²/N (3), and $^m s_{11} = 20 \times 10^{-12}$ m²/N (4). Curves (a), (b), and (c) correspond to $Lt^{-\frac{1}{2}} = 0.2$ m^½, 1 m^½, and 2 m^½, correspondingly

## 2.3  ME Coupling at Axial Mode of Electromechanical Resonance

Next we consider small-amplitude axial oscillations of the layered structures formed by magnetostrictive and piezoelectric phases. The displacement should obey the equation of media motion provided in Ref. [18]. To solve this equation, we used the boundary conditions for a bilayer that is free at both ends. Under assumption $^p K_{11}^2 \ll 1$, the fundamental EMR frequency is given by

$$f = \frac{1}{2L} \sqrt{\frac{^p s_{11} + r ^m s_{11}}{^p s_{11} {}^m s_{11} (r^p \rho + {}^m \rho)}} \tag{5}$$

and the peak ME voltage coefficient at axial mode frequency is

$$\frac{\delta E_3}{\delta H_1} = \frac{8 Q_a}{\pi^2} \frac{r ^m q_{11} {}^p d_{31} / {}^p \varepsilon_{33}}{(r ^m s_{11} + {}^p s_{11})(r + 1)} \quad \text{or}$$

$$\frac{\alpha_E}{Q_a} = \frac{8}{\pi^2} \frac{V(1 - V) {}^m q_{11} {}^p d_{31} / {}^p \varepsilon_{33}}{[V ^m s_{11} + (1 - V) {}^p s_{11}]} \tag{6}$$

where $Q_a$ is the quality factor for the EMR resonance.

It should be noted that Eqs. (5) and (6) for resonance frequency and ME voltage coefficient are valid for both bilayer and trilayer structures. It is easily seen from Eqs. (6), that the piezoelectric volume fraction dependence of ME voltage coefficient divided by Q value is similar to that of low frequency ME coefficient (Eq. 2). EMR frequency versus piezoelectric volume fraction is shown in Figs. 9 and 10.

## 2.4  ME Coupling in FMR Region

For calculating the electric field induced shift of magnetic resonance line, we consider a bilayer of ferrite and piezoelectric. The ferrite component is supposed to be subjected to a bias field $H_0$ perpendicular its plane that is high enough to drive the ferrite to a saturated state. Next, we use the law of elasticity and constitutive equations for the ferrite and piezoelectric and the equation of motion of magnetization for ferrite phase.

The shift of magnetic resonance field can be expressed in the linear approximation in demagnetization factors due to electric field induced stress [18]:

$$\delta H_E = -\frac{M_0}{Q_1} \left[ Q_2 \left( N_{11}^E - N_{33}^E \right) + Q_3 \left( N_{22}^E - N_{33}^E \right) - Q_4 N_{12}^E \right], \tag{7}$$
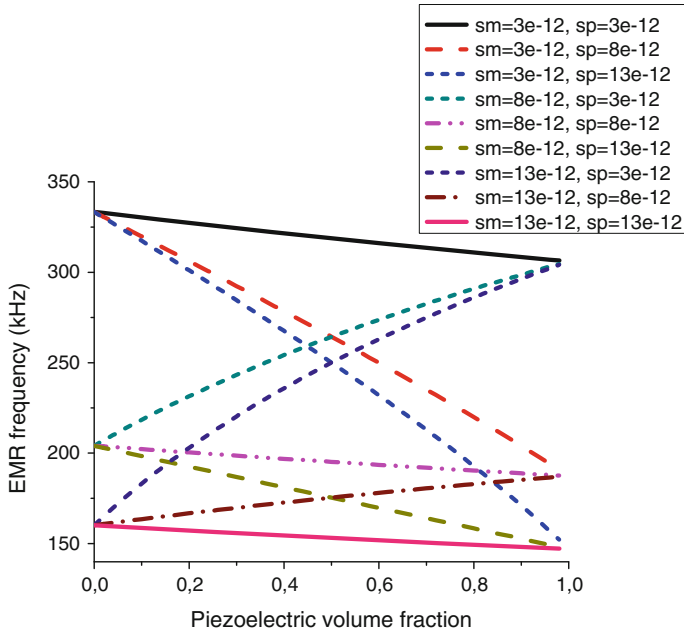
**Fig. 9** EMR frequency versus piezoelectric volume fraction for longitudinal mode of 10 mm long magnetostrictive-piezoelectric layered structure
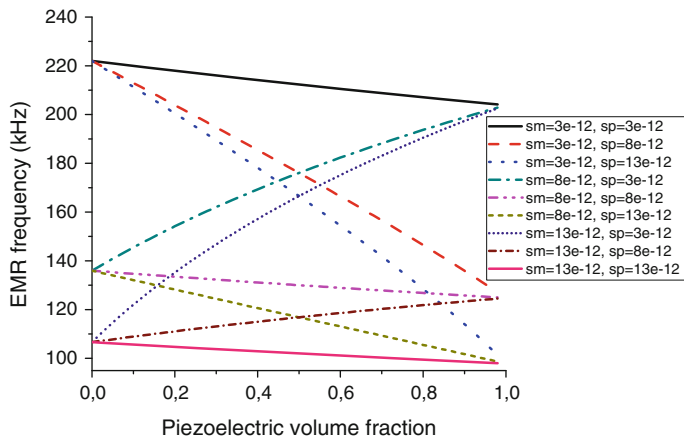


**Fig. 10** EMR frequency versus piezoelectric volume fraction for longitudinal mode of 15 mm long magnetostrictive-piezoelectric layered structure

where

$$Q_1 = 2H_3 + M_0 \sum_{i \neq E} \left[ \left( N_{11}^E - N_{33}^E \right) + \left( N_{22}^E - N_{33}^E \right) \right];$$

$$Q_2 = \left[ H_3 + M_0 \sum_{i \neq E} \left( N_{22}^i - N_{33}^i \right) \right];$$

$$Q_3 = \left[ H_3 + M_0 \sum_{i \neq E} \left( N_{11}^i - N_{33}^i \right) \right];$$

$$Q_4 = 2M_0 \sum_{i \neq E} N_{12}^i.$$

In Eq. 7, $N_{kn}^i$ are effective demagnetization factors describing the magnetic crystalline anisotropy field (i = a), form anisotropy (i = f), field and electric field induced anisotropy (i = E).

As an example, we consider a specific case of magnetic field $H$ along [111] axis. The shift of FMR field versus ferrite volume fraction is shown in Figs. 11. and 12. Electric field dependence of FMR field shift is presented in Fig. 13.

To obtain the estimates of ME coefficients from nomographs referred to above, one should use the material parameters of composite components. The relevant parameters of several materials that are most often used in ME structures are given in Table 1.



**Fig. 11** Ferrite volume fraction dependence of magnetic resonance line shift at E = 1 kV/cm for ferrite-piezoelectric bilayer for $\left| \frac{\lambda_{111}}{M_s} \right| = 0.16 \times 10^{-8}$ Oe$^{-1}$

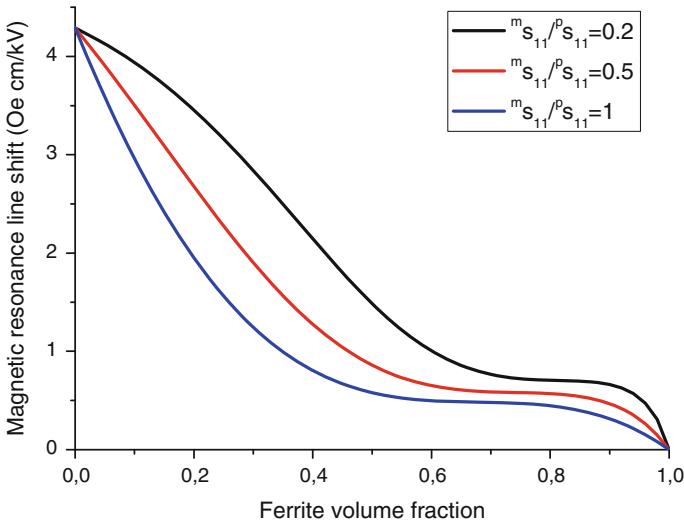**Fig. 12** Ferrite volume fraction dependence of magnetic resonance line shift at E = 1 kV/cm for ferrite-piezoelectric bilayer for $\left|\frac{\lambda_{111}}{M_s}\right| = 0.68 \times 10^{-8}$ Oe$^{-1}$



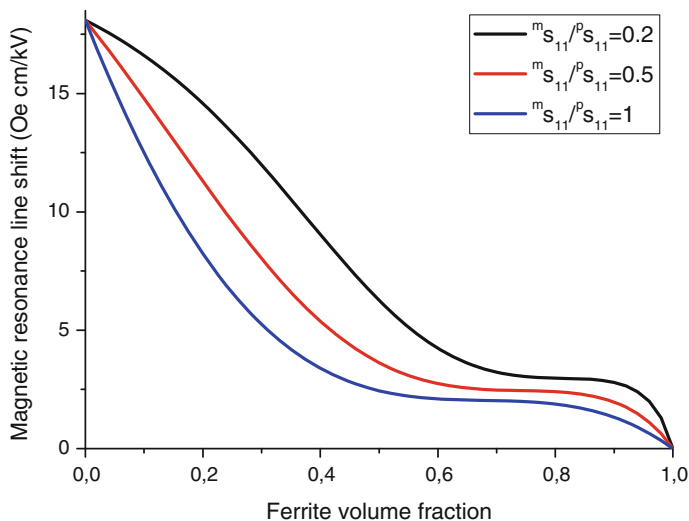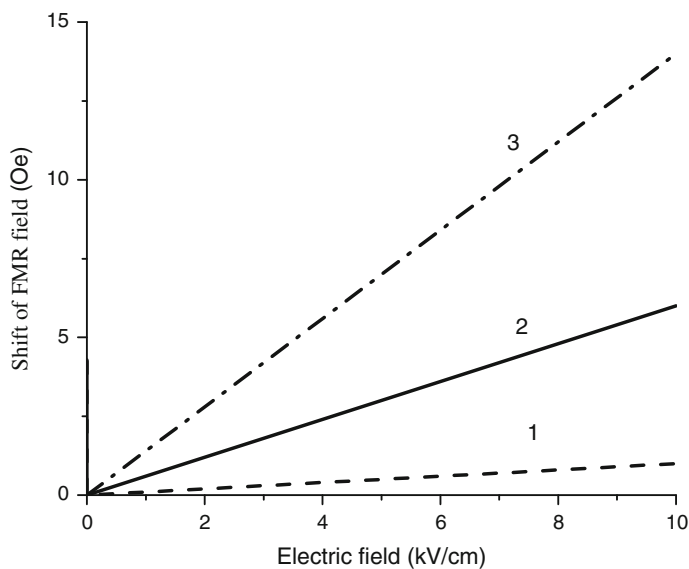**Fig. 13** Estimated shift of FMR field versus applied electric field at 9.3 GHz for the bilayers of YIG and PZT (*1*), NFO and PZT (*2*), and LFO and PZT (*3*) with equal thicknesses of magnetic and piezoelectric components

**Table 1** Material parameters for piezoelectric and magnetostrictive materials used for fabrication of layered structures

| Material | $s_{11}$ ($10^{-12}$ m²/N) | $s_{12}$ ($10^{-12}$ m²/N) | $q_{33}$ ($10^{-12}$ m/A) | $q_{31}$ ($10^{-12}$ m/A) | $d_{31}$ ($10^{-12}$ m/V) | $d_{33}$ ($10^{-12}$ m/V) | $\lambda_{100}$ ($10^{-6}$) | $\varepsilon_{33}/\varepsilon_0$ |
|---|---|---|---|---|---|---|---|---|
| PZT | 15.3 | −5 | – | – | −175 | 400 | – | 1750 |
| BTO | 7.3 | −3.2 | – | – | −78 | | – | 1345 |
| PMN-PT | 23 | −8.3 | | | −600 | 1500 | | 5000 |
| YIG | 6.5 | −2.4 | | | – | – | 1.4 | 10 |
| NFO | 6.5 | −2.4 | −680 | 125 | – | – | 23 | 10 |
| LFO | 35 | −12 | | | | | 46 | 10 |
| Ni | 20 | −7 | −4140 | 1200 | | | | |
| Metglas | 10 | −3.2 | 14000 | −3000 | – | – | | |

As an example of ME structure, we consider the bilayer of Ni and PZT with piezoelectric volume fraction 0.5. Based on data in Table 1, we get $^{m}s_{11} = 20 \times 10^{-12}$ m²/N, $^{p}s_{11} = 15.3 \times 10^{-12}$ m²/N, $^{p}d_{31} = -175 \times 10^{-12}$ m/V, $^{m}q_{11} = -4140 \times 10^{-12}$ m/A, $^{p}\varepsilon_{33}/\varepsilon_{0} = 1750$. Figure 4 at point A reveals the low-frequency ME voltage coefficient $\alpha_{E,31} = 190$ mV/(cm Oe). Then, Fig. 5 gives the peak ME voltage coefficient $\alpha_{E,31} = 20$ V/(cm Oe) at bending resonance frequency and Fig. 2 gives the peak ME voltage coefficient $\alpha_{E,31} = 70$ V/(cm Oe) at axial resonance frequency. Q-value is assumed to be equal to 100.

In the section we presented a new quick test of ME composites using nomographs and showed its application.

## 3 Magnetic Field Sensors

### 3.1 Background

A sensor is known to be a device that detects changes in quantities and provides a corresponding output. The magnetoelectric (ME) sensor represents a structure with ME coupling with two electrodes for connecting to the voltmeter. The action of the sensor is based on the magnetoelectric effect. A composite of magnetostrictive and piezoelectric materials is expected to be magnetoelectric since a deformation of the magnetostrictive phase in an applied magnetic field induces an electric field via piezoelectric effect.

The ME effect in composites of magnetostrictive and piezoelectric phase is determined by the applied dc magnetic field, electrical resistivity, volume fraction of components, and mechanical coupling between the two phases. The ME interaction is a result of magnetomechanical and electromechanical coupling in the magnetostrictive and piezoelectric phases, and stress transfer through the interface between these two phases. It should be noted that both the magnetomechanical response in magnetostrictive phase and electromechanical resonance in piezoelectric phases are possible origin of ME output peaks.

To obtain the maximal ME output, the bias and ac magnetic fields should be simultaneously applied to the sample. For measuring either of these fields, the value of second field should be specified. In an ac magnetic field sensor, the reference bias magnetic field can be generated by both permanent magnet and electromagnet [19]. Making a dc (ac) magnetic field sensor implies using the additional magnetic system to produce the ac (dc) reference field as in Fig. 14.

**Fig. 14** The equivalent circuit of ac (dc) magnetic field sensor. *1* and *2* are the ME composite sample and dc (ac) electromagnet
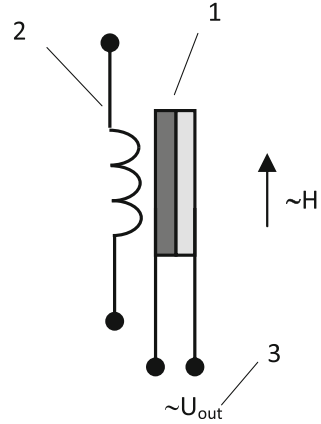
## 3.2 Physical Model

The static ME effect can be measured by using the electromagnet with Helmholtz coils between the electromagnet poles. The Helmholtz coils generate the dc magnetic field in the ME composite. Applying the dc magnetic field to the ME layered structure induces the output dc voltage across the piezoelectric layer. The relation between output voltage and magnetic fields can be described by sensitivity. The sensitivity of the ME sensor is determined by following expression: $S = \alpha_E \cdot {}^P t$ where $\alpha_E = \Delta E/\Delta H$ is ME voltage coefficient and ${}^P t$ is the piezoelectric layer thickness with $\Delta E$ and $\Delta H$ denoting the induced voltage and applied magnetic field.

The variation of static ME sensitivity, $(\Delta E/\Delta H)_H$, as a function of magnetic field H, at room temperature is shown in Fig. 15. It is observed that the sensitivity $S$ initially increases up to a certain magnetic field and finally attains a maximum

**Fig. 15** Theoretical ME voltage coefficient versus H and data for bilayer of NFO and PZT
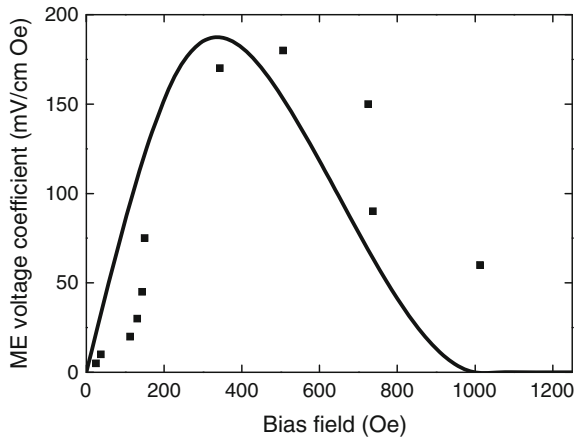
value and then decreases with an increase in applied dc magnetic field. This is because the magnetostrictive coefficient reaches saturation at a certain value of magnetic field. Beyond saturation the magnetostriction and the strain thus produced would also produce a constant electric field in the piezoelectric phase making the sensitivity decrease with increasing magnetic field.

The increases in $(\Delta E/\Delta H)_H$ with magnetic field is attributed to the fact that the magnetostriction reaches its saturation value at the time of magnetic poling and produces a constant electric field in the ferroelectric phase. Therefore, beyond a certain field, the magnetostriction and the strain thus produced would produce a constant electric field in the piezoelectric phase. Also, the possible reason for decrease in $(\Delta E/\Delta H)_H$ after certain magnetic field is attributed to the saturation state of the magnetic phase which does not show any response to the increased applied magnetic field therefore stress transfer through the interface between magnetic and electric phase decreases with magnetoelectric coupling $(\Delta E/\Delta H)$.

## 3.3 Noise Sources and Their Mitigation

Recent investigations of ME laminates sensors have shown that they have remarkable potential to detect changes in magnetic fields. It was shown that the feasibility of detecting magnetic field changes on the order of $10^{-12}$ T at near quasi-static frequencies of $f > 1$ Hz. This is an important achievement because the ME sensor does not itself require powering; rather it can harvest magnetic energy from inductances as a stored charge across a capacitor. Thus, ME laminates are small, passive magnetic field sensors with the potential of pico-Tesla sensitivity at low frequencies while operated at room temperature. The potential for ME sensors resides with the fact that there are no other present generations of magnetic sensors having the following key requirements [6, 20]: (i) extreme sensitivity ($\sim$pT/Hz$^{1/2}$), allowing for better magnetic anomaly detection; (ii) zero power consumption to foster long-term operation; (iii) operation at low frequencies, $f \sim 1$ Hz; (iv) miniaturize size, enabling deployment of arrays; (v) passive; and (vi) low cost. It should be noted that ME laminate sensors are the only ones with the potential to achieve all key requirements. However, in spite of this potential, there are no available technologies that can fulfill requirements referred to above. The integration of ME laminates into an appropriate detection scheme has yet to be achieved. This detection scheme must be simple and capable of detecting anomalies in the time domain capture mode without either signal averaging or phase referencing.

Commonly, noise is defined as any undesirable disturbance that obstructs the relevant signal passage. It is of importance in the measurement of minute signals. Reducing the noise effect on the detection device is important since the sensitivity of a sensor is often limited by noise level. We will consider some simple ways to reduce noise.

The sensor itself and the measurement circuit contribute some inherent noise. This kind of noise cannot be removed since it comes from stochastic phenomena: thermal and radiation fluctuations between sensor and environment, generation and

recombination of electron-hole pair, and current flows across a potential energy barrier in materials.

Development in the noise reduction of magnetostrictive/piezoelectric laminate sensors has been carried out in the past decade. Particularly, a 1 Hz equivalent magnetic noise of 5.1 pT $Hz^{-1/2}$ has been obtained, which is close to that of the optically pumped ultralow magnetic field sensors [21]. First of all, this was enabled by improved methods of interfacial bonding that can decrease the equivalent magnetic noise floor up to $2.7 \times 10^{-11}$ T $Hz^{-1/2}$ [22]. Then, optimal poling conditions for the piezoelectric phase result in an increase in ME voltage coefficient by a factor of 1.4. The equivalent magnetic noise at $f = 1$ Hz was reported to equal 13 to 8 pT $Hz^{-1/2}$ [23].

Magnetic flux concentration was found to enhance the ME coefficient of an ME sensor. A dumbbell-shaped sensor with an enhanced ME coefficient and reduced equivalent magnetic noise was reported [24], in which the dumbbell shape leads to concentration of magnetic flux. ME laminates with dumbbell-shaped Metglas layers exhibited 1.4 times lower required dc magnetic bias fields and 1.6 times higher magnetic field sensitivities than traditional rectangular-shaped ME laminates.

It was found that Mn-doped PMN-PT single crystals have the advantages of high piezoelectric coefficient and extremely low tan $\delta$. Experimentally, an ultralow equivalent magnetic noise of 6.2 pT $Hz^{-1/2}$ was obtained at 1 Hz of the multi-push–pull mode for Metglas/PMN-PT single crystals [25].

## 3.4   Fabrication

The combination of magnetostrictive amorphous ferromagnetic ribbons with piezoelectric materials, allows obtaining magnetoelectric laminated composites, that show an extremely high sensitivity for magnetic field detection. Magnetic alloys epoxyed to Polyvinylidene Fluoride (PVDF) piezoelectric polymer give as result magnetoelectric coefficients above 80 V/cm Oe. Also, high temperature new piezopolymers as polyimides are can be used for the magnetoelectric detection at temperatures as high as 100 °C.

ME three-layer can be constructed sandwich-like with longitudinal magnetostrictive operation and transverse piezoelectric response laminated composites by gluing two equal magnetostrictive ribbons to opposite sides of polymer piezoelectric films with an adhesive epoxy resin [6]. Magnetostrictive ribbons belonging to the family of Fe–Co–Ni–Si–B, Fe-rich metallic glasses have a measured magnetostriction that ranges between $\lambda s \approx 8$–30 ppm and maximum value for the piezomagnetic coefficient $d_{33} = d\lambda/dH$ of about $0.6$–$1.5 \times 10^{-6}$/Oe. This last parameter will modulate the magnetoelectric response of the composite as a function of the applied bias magnetic field. Concerning the piezoelectric material we firstly used the well-known polymer PVDF, the well-known piezoelectric polymer, with glass transition and melting temperatures about −35 and 171 °C, respectively, but a Curie temperature of ≈100 °C. This makes its piezoelectric

response to decay quickly above 70 °C. To develop a ME device being able to operate at higher temperatures, new amorphous piezoelectric polymers of the family of the polyimides were tested. It should be noted that its main parameters are a glass transition temperature of $Tg \approx 200$ °C and a degradation temperature of $Td \approx 510$ °C, temperatures that make these polyimides suitable for our purposes. Taking advantage of the magnetoelastic resonance effect that enhances the magnetostrictive response, all measurements have been taken at resonance. For that, the static magnetic field $H_{DC}$ necessary to induce the maximum amplitude of that resonance was first determined. The induced magnetoelectric voltage in the sandwich laminate (through two small silver ink contacts located at both opposite magnetostrictive ribbons) was measured by the following procedure: under a $H_{AC}$ magnetic excitation applied along the length direction, the magnetostrictive ribbons will elongate and shrink along the same direction. This will make the piezoelectric polymer film to undergo an ac longitudinal strain, inducing a dielectric polarization change in its transverse direction. Thus, we can determine simultaneously the ME response dependence as the bias field $H_{DC}$ changes; and at the $H_{DC}$ value for the maximum magnetoelastic resonance amplitude, the ME voltage dependence vs the applied ac magnetic excitation.

The highest ME response has been reported for laminated magnetostrictive/piezoelectric polymer composites. ME voltage coefficient of 21.5 V/(cm Oe) for a METGLAS 2605 SA1/PVDF (Metglas, Conway, SC, USA) laminate was achieved at non-resonance frequencies and is, so far, the highest response obtained at sub-resonance frequencies [6]. At the longitudinal resonance mode, energy transference from magnetic to elastic, and vice versa, is maximum. This energy conversion at the resonance turns out to be very sharp for ME laminates, while frequency bandwidth for applications based in this EMR enhancement effect remains limited. ME voltage coefficient of 383 V/(cm Oe) on cross-linked P (VDF-TrFE)/METGLAS 2605 SA1 is the highest reported to date. In order to avoid the observed sensitivity decrease when increasing temperature, the same L-T structured magnetoelectric laminates was fabricated with the same magnetostrictive constituents but using a 40/60 copolyimide as high temperature piezoelectric constituent.

Efforts to get wider bandwidths for EMR and ME applications have been mainly based on magnetic field tuning procedures either in bimorph or tri-layered structures, but the maximum achieved frequency of operation has been some tenths of kHz. Another way to get high frequencies of operation can be based on the relationship between length and resonant frequency value of magnetostrictive ribbons at the magnetoelastic resonance. So, our efforts are now focused on fabricating short magnetoelectric L-T type laminates showing good magnetoelectric response at high frequencies. Nevertheless, the higher the resonant frequency the lowest the amplitude of the resonance and as a first consequence, the magnetoelectric response will be also decreased. It is clear that a compromise between length of the device and so working frequency, and induced magnetoelectric signal, must be achieved. Thus, a device 1 cm long for which the resonant (working) frequency rises to 230 kHz was developed. The measured magnetoelectric voltage coefficient is about

15 V/(cm Oe) when PVDF is used as piezoelectric constituent. Thus a 0.5 cm long device that will work at a resonant frequency about 500 kHz is expected to be constructed. This fact, combined with the use of a high temperature piezopolymer as the polyimides previously described, can lead to a very useful class of magnetoelectric laminates working simultaneously at high temperature and within the radiofrequency range, both characteristics of great interest for low distance near field communications in aggressive environments (i.e., the desert, a tunnel or fighting a fire).

Combining the excellent magnetoelastic response of magnetostrictive amorphous ferromagnetic ribbons with piezoelectric polymers, the short length magnetoelectric laminated composites that show an extremely high sensitivity for magnetic field detection was fabricated.

## 3.5   Review of Recent Results

The magnetic sensors based on magnetoelectric composites for the practical purposes including the use in biomagnetic imaging have been of considerable interest in recent years [26–37]. Migratory animals are capable of sensing variations in geomagnetic fields as a source of guidance information during long-distance migration. It is well known that geomagnetic fields are on the order of 0.4–0.6 Oe and have different inclinations at different locations. The Earth's mean field and its inclinations at many points over much of the Earth's surface are known to be tabulated. Accordingly, geomagnetic field sensors could be used in guidance and positional location. There are many types of magnetic sensors: for example, superconducting quantum interference devices or giant magnetoresistance spin valves. However, these sensors require very low operational temperatures liquid nitrogen in order to achieve high sensitivity. Fluxgate sensors based on exciting coil have been investigated for many years to detect dc magnetic and geomagnetic fields. This widely used sensor is relatively cheap and temperature independent; however, its magnetic hysteresis, offset value under zero magnetic field, and large demagnetization factor restrict design considerations. Recently, new types of passive ac and active dc magnetic field sensors have been developed based on a giant magnetoelectric ME effect. They are simple devices that work at room temperature. The laminated composites, such as magnetostrictive Terfenol-D or ferrite layers together with Pb $Zr_{1-x},Ti_x$ $O_3$ PZT ones, have been found to possess giant ME effects of between 0.1 and 2 V/cm Oe under dc magnetic bias of $H_{dc} < 500$ Oe. Furthermore, a larger ME coefficients of up to 22 V/cm Oe under $H_{dc} < 5$ Oe have recently been reported for Metglas/PZT-fiber laminates at quasistatic frequency, which is 10 times larger than prior reports for laminates and $10^4$ times larger than that of single phases. As a result, using a Metglass/PZT-fiber ME sensor enables one to detect precisely both geomagnetic fields and their inclinations along various axes of a globe. This ME sensor is a Metglas/PZT-fiber laminate with a 100 circle coil wrapped tightly around it. The PZT fibers were 200 μm in thickness and were

laminated between four layers of Metglas by use of a thin layer epoxy; the thickness of each Metglas layer was 25 μm, and the total dimensions of the laminates were $100 \times 6 \times 0.48$ mm³. The working principal of the ME sensor is that an input magnetic field changes the length of the Metglas via magnetostriction, and because the PZT fibers are elastically bound to the Metglas layers through an epoxy interfacial layer, the PZT fibers also change their length and generate an output voltage via piezoelectricity. Detection of the Earth's magnetic field was performed by applying a 1 kHz ac magnetic field $H_{ac}$ via a 10 mA ac input to the coil and by measuring the dc voltage and its phase induced in the PZT fibers by a lock-in amplifier SR-850. Over the range of $-1.5 < H_{dc} < 1.5$ Oe, $V_{ME}$ was linearly proportional to $H_{dc}$ and equal to 300 mV under a $H_{dc} = 1$ Oe. This value is $10^3$ times as large as that of a corresponding Terfenol-D/PZT dc magnetic field sensor operated at 1 kHz. Another important finding was that, unlike Terfenol-D/PZT magnetic sensors, $V_{ME}$ for Metglas/PZTfiber sensors was not dependent on $H_{dc}$ history (i.e., no hysteretic phenomena). This is very important to a stable and repeatable detection of dc magnetic fields and their variations. In addition, when the sign of $H_{dc}$ was changed, a dramatic 180° phase shift was found. This shift could be used to distinguish the direction along which changes in $H_{dc}$ occur with respect to the length long axis of the sensor. This is an important advantage compared to fluxgate. Previously, it was reported that $V_{ME}$ from a Metglas/PZT fiber laminates was strongly anisotropic, offering good sensitivity to magnetic field variations only along its length direction. In the other two perpendicular directions, only very weak signals were found with changes in $H_{dc}$. These unique properties of Metglas/PZT-fiber ME sensors are due to the ultrahigh relative permeability $r$ of Metglas, which is $10^3$ times larger than that of Terfenol-D or nickel ferrite. Correspondingly, the high $r$ of Metglas results in an ultrasmall demagnetization field, enabling a high effective piezomagnetic coefficient at low biases.

Thus sensitivities of a few pico-Tesla to hundreds of femto-Tesla for 1–30 MHz magnetic fields are required for use in biomagnetic imaging. A possible approach for achieving such sensitivities is a bilayer ME sensor operating under frequency modulation at bending resonance [6]. It is of interest to compare the low-frequency and resonance ME voltage coefficients in representative bilayer composite systems. One of the best values for low-frequency ME voltage coefficient, $\sim 52$ V/cm Oe, was measured in samples of Metglas and a piezofiber and was attributed to high $q$ value for Metglas and excellent magnetic field confinement field due to high permeability. A recent study that compared the low-frequency and resonance ME effects in bilayers of composites with permendur and ferroelectric PZT and PMN-PT and piezoelectric langatate and quartz [36]. The highest ME voltage coefficient of 1000 V/cm Oe at bending resonance among these systems was measured for a permendur-langatate bilayer. But the highest resonance ME voltage coefficient to-date, 20 kV/cm Oe, was reported for AlN-FeCoSiB for measurements under vacuum that reduces damping of bending resonance in air [26, 27]. A very high ME sensitivity was also reported under bending resonance in a cantilever of FeCoSiB and PZT with inter-digital electrodes.

**Table 2** Properties of modern magnetic field sensors [6, 20]

| Sensor type | Sensitivity (at 1 Hz) (Tesla/Hz$^{1/2}$) | Measuring mode |
|---|---|---|
| High-temperature superconducting quantum interference devices (SQUID) | $5 \times 10^{-14}$ | T < 77 K |
| Giant magnetoresistance (GMR) spin valve | $4 \times 10^{-10}$ | T = 300 K<br>I = 1 mA |
| Hybridizing a GMR sensor with a superconducting flux-to-field transformer | $10^{-12}$ | T = 77 K<br>I = 5 mA |
| Chip-size atomic magnetometer | $5 \times 10^{-11}$ | f = 10 Hz |
| Magnetoelectric magnetometer | $3 \times 10^{-11}$<br>$2 \times 10^{-15}$ | T = 300 K<br>T = 300 K at resonance frequency ($10^{5 \text{ Hz}}$) |

ME sensitivity optimization should take into account the environmental or external noise sources, such as thermal fluctuation and mechanical vibration. These external noises will be dominating factors that affect the sensor's sensitivity in practical applications. For ME sensors, the dominant ones are the thermal fluctuation and mechanical vibration sources. Thermal fluctuation noise is pyroelectric in origin, where the spontaneous polarization of the piezoelectric phase is temperature dependent, resulting in a dielectric displacement current in response to temperature changes; whereas the vibrational noise is piezoelectric in origin, where the spontaneous polarization is coupled to pressure and stress changes, via piezoelectricity. As for all magnetic field sensors, it is important that ME sensors be designed by such a means that optimizes its abilities to cancel these external noise.

Comparative characteristics of modern magnetic field sensors are presented in Table 2.

In the case of the push-pull laminate, the extreme enhancement in the sensitivity limits ($\sim 10^{-15}$ T/Hz$^{1/2}$) at EMR is nearly equivalent to that of a SQUID sensor operated a 4 K and 15 mA.

ME laminates offer much potential for low frequency $10^{-2}$–$10^{3}$ Hz detection of minute magnetic fields ($10^{-12}$ T or below), at room temperature, in a passive mode of operation, such combinations of characteristics are not available in any other magnetic sensor.

# 4 Current Sensors

## 4.1 Background

Current sensors are very essential kind of product. There are many different types of sensors that are designed on different physical principles. The most common types of sensors have been developed on the use of a resistive shunt, current transformer,

magnetoresistance and Hall sensor. A new type of sensors on ME effect has good isolation, it has small dimensions and weight and at the same time, a significant advantage in sensitivity. Different variants of designs have been investigated. Operating principle of ME current sensor is based on measuring the electromagnetic field generated by current [38]. The value of the electromagnetic field allows one to estimate the magnitude of the current flowing in the conductor. Next, the use of ring-type magnetoelectric laminate composites of circumferentially magnetized magnetostrictive Terfenol-D and a circumferentially poled piezoelectric Pb(Zr,Ti) $O_3$ (PZT) which have high sensitivity to a vortex magnetic field is suggested [39–41]. At room temperature, an induced output voltage from this ring laminate exhibited a near-linear response to an alternating current (ac) vortex magnetic field $H_{ac}$ over a wide magnetic field range of $10^{-9} < H_{ac} < 10^{-3}$ T at frequencies between sub-Hz and kHz. A significant improvement of sensors sensitivity for this type devices through the use of current transduction mode was proposed in [42]. Such a sensor, according to a study [43] has an increased sensitivity to ultra-low magnetic fields and leakage currents. This circumferential-mode quasiring ME laminate can detect AC currents (noncontact) $10^{-7}$ A, and/or a vortex magnetic field $6 \times 10^{-12}$ T. Next, a self-powered current sensor consisting of the magnetostrictive/piezoelectric laminate composite and the high-permeability nanocrystalline alloys is presented in [44]. However, this design can measure only ac current, which significantly limits its use. Next, we consider the dc current sensor based on ME element with the modulating coil.

The ME current sensor uses the ME effect as a basis of its measurements. The ME effect is a polarization response to an applied magnetic field, or conversely a magnetization response to an applied electric field. ME behaviour exists as a composite effect in multiphase systems of piezoelectric and magnetostrictive materials. Magnetostrictive-piezoelectric laminate composites have much higher ME coefficients than that of single-phase materials or particulate composites. In a magnetostrictive-piezoelectric layered structure the interaction between magnetic and electric subsystems occurs through mechanical deformation. It means that the ME effect is much stronger at frequencies corresponding to elastic oscillations called resonance frequencies. In current sensor applications the induced ME voltage coefficient is more important than the induced ME electric field coefficient, as voltage is the physical quantity measured. The sensor is designed for detecting ac and dc currents in electrical circuits [45–47] on range from 0 up to 1, 10 or 100 A depending on destination.

ME current sensors can be designed on different principles. In the first case, the operation principle work of ME element is nonresonant, in the second case the principle is resonance. As a sensitive element of the sensor in both cases can used the same design of ME element. The design of nonresonant ME current sensors was considered in the paper [45], and the design of resonant ME current sensors in the paper [46, 47]. An input-to-output ME current sensor was also developed, which includes the internal current conductor as a source of information about the current, and a surface-mounted sensor placed directly on the conductor with the current to be measured. We consider here the basic principles of work of ME current sensors of non-resonant type based on the low-frequency ME effect and next the resonant

type, working on one excited in the piezoelectric phase of magnetoelectric material of a resonant electromechanical oscillations. Also there are ac and dc ME sensors. ME ac current sensor is a special case of the direct current sensor, as it doesn't contain the modulating coil and generator and, therefore, simpler to manufacture. ME dc sensor can operate as an ac sensor without design modification.

## 4.2 Physical Model

The equivalent circuit of the device is represented in Fig. 16. The principle of operation of the sensor is based on measuring the potential appearing at the output of ME element due to ME effect under the influence of external modulation magnetic fields and bias magnetic field. ME sensor dc will differ from the ME sensor ac only additional baseband generator.

We can carry out modeling of current sensor using known basic formula of electrophysics and using an expression for determine of ME coefficient. When the solenoid is included into the structure of current sensor, the well-known expression for the calculation of the magnetic field inside the solenoid can be used:

$$H = \frac{N \cdot I}{l} \tag{8}$$

where $H$ is magnetic field inside the solenoid, $I$ is measured current in the conductor, $l$ is the length of the solenoid, $N$ is the number of turns of the solenoid.

Let us write the expression for the ME coefficient, expressing the intensity of the electric field:

$$E = H \cdot \alpha_E \tag{9}$$



**Fig. 16** The equivalent circuit of ME dc current sensor. *1* is ME element, *2* is ac solenoid coil, *3* is dc solenoid coil for measurement dc current
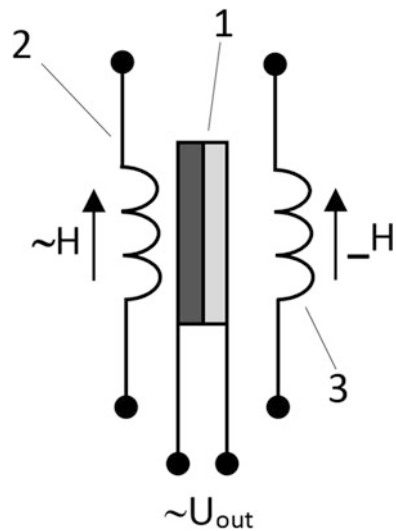
where is ME coefficient, $E$ is intensity the electric field in ME material. Due to the ME effect, an electric potential equal to $U = dE$ appears across the ME element, where $d$ is piezoelectric thickness. The expression (8) we substitute in (9) and obtain, respectively:

$$U = \alpha_E \frac{N \cdot I \cdot d}{l} \qquad (10)$$

If in scheme of current sensor an amplifier is used, then in the expression should include the gain factor $K_g$ and the measured current is expressed in terms of output voltage of the sensor as follows:

$$U_s = K_g \alpha_E \frac{N \cdot I \cdot d}{l} \qquad (11)$$

The coefficient $\alpha_E$ depending on the operation mode can be written for different cases: nonresonant case for bending mode, for operation at the longitudinal resonance, for a thickness resonance.

According to expression (11) output voltage directly proportional to the flowing current and number of turns of the solenoid and is inversely proportional to the magnetic permeability of ME composite. The design of ME sensor was developed on the basis of these theoretical positions. Estimation of the parameter Us gives the result: when $N = 500$, $I = 1.2$ A, $d = 3$ mm, $l = 10$ mm, $\alpha_E = 2.5$ V/A, $K_g = 10$, then we obtain the output voltage equal to 4.5 V, which is in good agreement with experiment.

## 4.3 Fabrication

The design of ME sensor in the general case consists of a driver and a measuring head which includes ME element. The scheme of driver depends on the required measurement.

### 4.3.1 ME Element

ME element is the sensitive part of ME current sensor and consists, for example, of piezoelectric and magnetostrictive layers as shown in Fig. 17. Layered structure based on piezoceramic PZT plate in this case had 0.38 mm of thickness, 10 mm of



**Fig. 17** Structure of ME element: (*1*) is PZT, (*2*) is Metglas, (*3*) is ME element

length and 1 mm of wide was investigated in [45]. Piezoelectric was polarized in the thickness direction. The electrodes are applied on two sides of the piezoelectric plate. The electrodes are made from three layers of Metglas and correspond in size the PZT plate. Thickness of one layer of Metglas was about 0.02 mm. Joint of layered design was done by gluing. Various types of adhesives including epoxy glue can be used. In general case, several piezoelectric plates instead of one can be used to increase the sensitivity. Also number of Metglas layers may be different in dependence on the required sensitivity. The electrical signal is taken from the surface of Metglas plates.

### 4.3.2 Measuring Head

Measuring head is an important element of the sensor shown in Fig. 18. ME element is placed in the inductance coil where a permanent magnetizing field and a variable modulation magnetic field are created.

   Bonding the ME element to the coil inductance is very important. ME element must be fixed at one end only to avoid pinching magnetostrictive layer on the rest of the surface element. Also there is a current coil as shown in Fig. 18.

### 4.3.3 Sensor Schematic

In nonresonant case the scheme of current sensor consists of a generator that is tuned to the frequency, for example, about 500 Hz. Generator is connected to the inductance coil for generation of magnetic modulation field and then the signal from the ME sensor leading-out wires is amplified and fed to a peak detector. Current coil creates a constant magnetic field proportional to the current strength. If it is required, sensor's circuit can contain a microprocessor with internal analog-to-digital converter for signal conversion. Block diagram of dc sensor is shown in Fig. 19. In resonant case the scheme of current sensor similar with one, but sensitivities of the scheme some more about from ten to hundred times.



**Fig. 18** Design of ME sensor measuring head: (*1*) is inductance coil, (*2*) is ME element, (*3*) is leading-out wire of ME element, (*4*) is glue, (*5*) is current coil
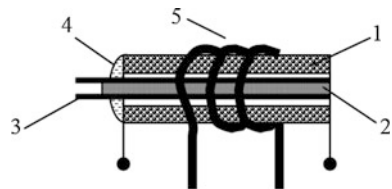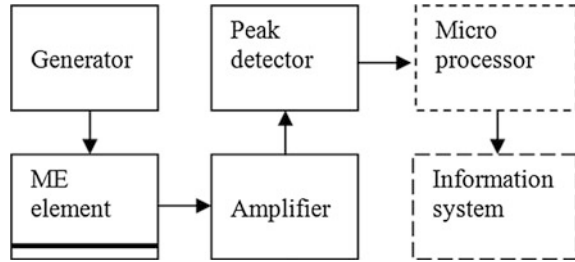
**Fig. 19** Block diagram of dc sensor



### 4.3.4 Construction

ME current sensor is a system consisting of ME element, generator, rectifier (or peak detector), permanent magnet, two coils one of which is wound on another and case. The construction of the dc ME sensor is presented in Fig. 20.

The design of ac sensors is similar to that of electromagnetic field. The difference between these types of sensors is that the ac sensor is mounted near the conductor with alternating current around which is formed an alternating magnetic field. A dc sensors can also be used as ac sensors. The sensitivity of such sensors will depend on ME material properties and ac current frequency, because the amplitude-frequency

**Fig. 20** Design of ME current sensor's prototype: **a** nonresonant sensor, **b** resonant sensor. (*1*) Is leading-out wire for detected current, (*2*) is current coil, (*3*) is ME element, (*4*) is the chipset case, (*5*) is generator, (*6*) is amplifier
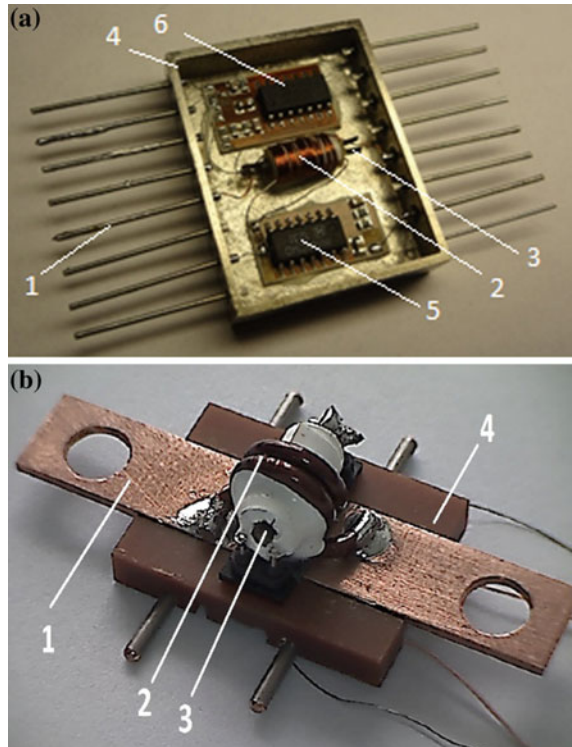
characteristic of the ME element is non-linear and strongly depends on the frequency. The maximum sensitivity of sensors will be at various resonant frequencies, and just below that, in the low frequency range are mostly up to several kHz. To increase the accuracy, it is necessary to choose materials with the lowest magnetic hysteresis loop.

### 4.3.5 Electronics

Standard instruments used in measuring bench are the regulated power supply and the oscilloscope. The measurement setup includes two power supplies APS-7315 (Aktakom), multimeter HM 8112-3 (HAMEG instr.), oscilloscope ACIP-4226-3 (Aktakom) and an electromagnet, Fig. 21. First power supply provides a constant current for measurement, the second provides power supply measurement scheme, oscilloscope or multimeter is necessary for control the output voltage.

### 4.3.6 Measurement Data

ME element includes piezoelectric PZT layer with dimensions $10 \times 5 \times 1$ mm and several layers of Metglas was researched and performed to optimize the sensor design.

ME element characteristics modulated by output voltage depending on the generator's frequency at the magnetic field of 3 mT is shown in Fig. 22. The curve has a non-linear form, with maxima at 1000 Hz and at electromechanical resonant frequency about 176 kHz. The resonance frequency depends on the linear dimensions of the element.

Data in Fig. 22 enable one to choose the oscillator frequency for the bias coil.

Characteristic of ME element output voltage depending on the magnetizing field at the frequency of 500 Hz is shown in Fig. 23. ME element characteristic has a strong maximum at bias field of 5 mT. The use of the linear characteristic part located from 0.5 to 4.5 mT or part from 6 to 8 mT is possible for the development of current sensors. We selected the first part for minimizing the magnetizing field.

Using data in Fig. 23 is convenient to choose the area in which will be carried out measurements of dc. For the development of the current sensor can be choose different zones of represented curve. For example, areas with the better linearity,

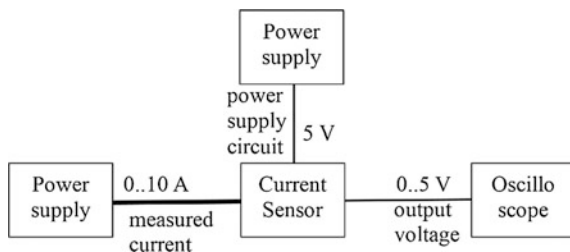**Fig. 21** Setup for measurement of dc current sensors

**Fig. 22** ME element characteristic modulated by output voltage depending on the generator's frequency at the magnetizing field of 3 mT
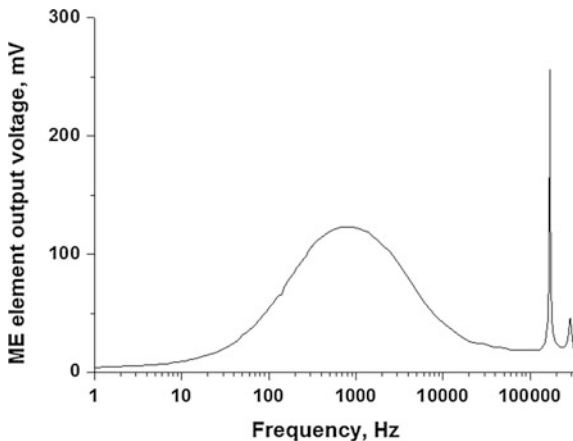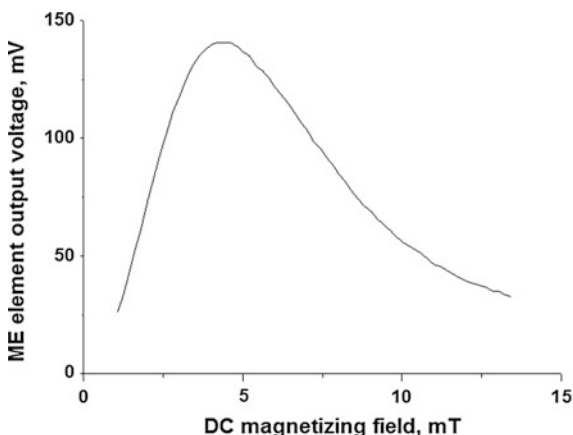


**Fig. 23** Characteristic of ME element output voltage depending on dc field at the frequency of 500 Hz



starting from 0.5 to 2.5 mT, then from 6 to 8 mT and finally, one can choose a non-linear areas and use methods of compensation or transformation.

For development ME current sensor important the choice of the optimal ME structure. Theoretical modelling of symmetric and asymmetric ME structures is discussed in detail in [48]. After selecting the optimal of ME structure can start the measurement characteristics of ME sensor.

The output signal can be adjusted picking up the desired number of turns in current coil. Using the different number of current coil turns to increase the output signal in addition to the amplifier is possible. The magnetic field applied to ME element will more strong at increasing the current coil turns, and accordingly, will more big output voltage from ME element. Graph of the current sensor output voltage depending on the measured constant field and different number of the current coil turns is shown in Fig. 24. Current sensor can be used on different level of current depending on the number of turns of the current coil. In addition, sensitivity to direct current can be adjusted by using the gain of the amplifier.

**Fig. 24** Current sensor output voltage depending on direct current and different number of the current coil turns (from 1 to 10)
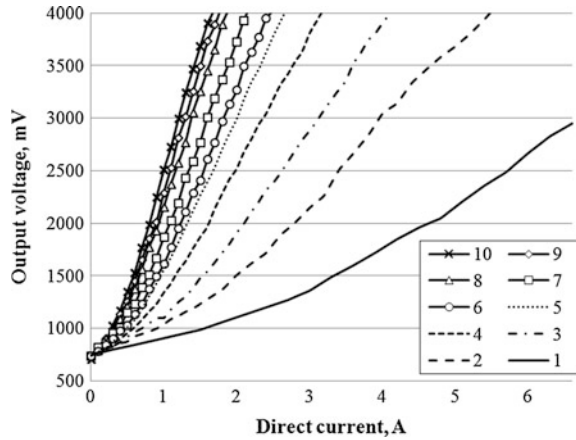


For the developed sensors the sensitivity of 1 A sensor is bigger than 3 V/A, for 5 A sensor sensitivity is about 0.68 B/A. The linearity of characteristic is within 1 %. Current consumption of the sensor is 2.5 mA. The increase in the number of coil current turns raises the sensitivity to the current. The sensor's design for a certain current can be calculated using the ratio of turns and sensitivity of the sensor.

The Table shows the dc sensors data. The information about the sensors HO8-NP production of LEM Holding SA, CSLW6B5 produced by Honeywell Inc., TLI4970 production of Allegro MicroSystems and also data of ME sensor discussed in [8] are presented in the table. ME sensors have higher sensitivity and lower current consumption compared to traditional sensors as it is evident from the Table 3 data.

**Table 3** Comparative characteristics of dc sensors

| Sensor features | HO8-NP | CSLW6B5 | ACS712ELCTR-05B-T | Magnetoelectric sensor |
|---|---|---|---|---|
| Measuring principle | Hall effect measuring principle | Miniature ratiometric linear Hall-effect sensor | Hall-effect sensor | Magnetoelectric effect |
| Primary current, measuring rang $I_{PM}$ (A) | 0–20 | ±5 | ±5 | 0–5 |
| Sensitivity (V/A) | 0.1 | 0.2 | 0.185 | 0.68 |
| Supply voltage (V) | 5 ± 10 % | 4.5–10.5 | 5 ± 10 % | 5 ± 10 % |
| Current consumptions (mA) | 19 | 9 | 10 | 2.5 |
| Accuracy (%) | 1 | 0.5 | 1.5 | 1 |
| Output voltage range $U_{out}$ (V) | 2.5–0.5 | 2.7–3.7 | 2.5–4.5 | 0.7–4.1 |
| Size in mm | 24 × 12 × 12 | 16.2 × 14 × 10 | 6 × 5 × 1.75 | 30 × 20 × 10 |

**Fig. 25** Current sensor
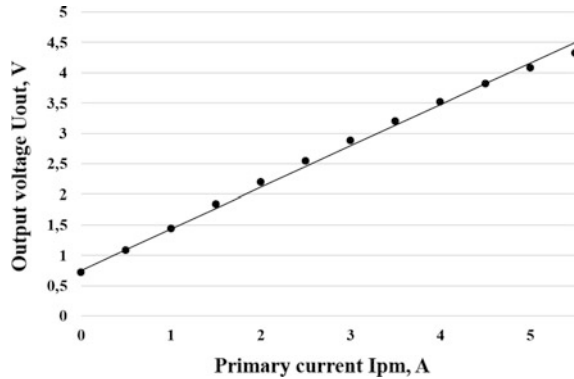output voltage depending on
dc



Figure 25 shows the characteristic of the dc current sensor for current up to 5 A.

In the future designs using of gradient ME materials and sensors placed directly on electric conductor will be explored. Using the layered structures based on compositionally graded materials enables making the sensors that can operate with no bias magnetic field applied [48]. Development of new highly sensitive ME materials will allow to develop industrial sensors are easily mounted on any surface without changing the design of the measured devices. Integrated ME sensors using MEMS or semiconductor technology in the future will also be developed.

## 5 Microwave Power Sensors

Almost all microwave devices use the sensor to measure any physical value that typically converts microwave oscillations in the measured signal. The operating principle of the majority of microwave power meters, called wattmeter's, is based on measuring changes in temperature or resistance elements in which the energy of electromagnetic oscillations is dissipated.

### 5.1 Measurement of Powerful Microwave Signal

There are various sensors for measuring the microwave power.

The calorimeters are used to measure power in the range from a few milliwatts to several hundred kilowatts. The principle of operation concludes in the equivalent conversion of electromagnetic wave energy into thermal energy calorimetric body, usually this is a water. Bolometers and thermistors: their operation is based on the transformation of the incident power into heat and the changing in resistance of the resistive element that is sensitive to temperature. Detector diodes are used for power up to 100 kW, operating range up to 100 GHz. Hall elements are used as a

walk-through power sensors in the microwave range. Meters with an absorbing wall: the principle of operation is based on the absorption of microwave power in the waveguide walls as a sensing element used semiconductor. Work of ponderomotive wattmeter is based on the mechanical action of the electromagnetic field on the conductor. Electron-beam method (Thomas method) is based on the interaction of the electron beam and the microwave field.

The disadvantages of such sensors include: non-linearity in strong magnetic fields, narrow dynamic and frequency range, a limited range of operating temperatures, the need for the voltage supply, the presence of residual stresses, low resistance to static electricity and radiation exposure [49, 50, 51, 52]. One of the most promising ways to improve the microwave power sensors is the use of ME material [12, 53]; the use of which allows to improve the performance of devices, expand their functionality and, in some cases, to create sensors with properties which are unobtainable in other types of sensors.

## 5.2   Equivalent Circuit

Sensors based on the ME materials have a wide frequency range from dc to tens of gigahertz, stable when exposed to significant levels of radiation, temperature range from 0 K to the Curie temperature of used components. ME composite materials consist of magnetostrictive and ferroelectric phases [15]. By selecting a certain of the original components in such systems it can be obtained ME interaction, sufficient for practical application. ME microwave power sensors are based on the resonant circuit [54].

For engineering calculations of resonant devices is a convenient method of analysis, in which the transmission line and the microwave resonator is considered as a bound system. The degree of coupling is characterized by a coefficient which presents the main characteristics of the transmission line with resonator: coefficient of reflection, transmission and absorption of electromagnetic microwave energy. The problem is solved in two steps: first, it is need to solve the equation of power balance (either by analyzing the equivalent circuits), that give us general expressions for the characteristics of the transmission line with resonator. Then, the coupling coefficients calculated for specific cases of resonator location in a microwave transmission line. Thus consider two types of losses: heat losses and reemission losses of electromagnetic energy in the transmission line.

Resonator quality factor Q, which is determined only on the basis of heat loss is own quality factor, reemission loss and loaded quality factor of the ME resonator are calculated as follows:

$$Q_0 = \frac{\omega W}{P_T}; Q_c = \frac{\omega W}{P_c}; \frac{1}{Q_L} = \frac{1}{Q_0} + \frac{1}{Q_c} \tag{12}$$

Fig. 26 The equivalent
circuit of the resonator which
is an element of coupling of
transmission lines
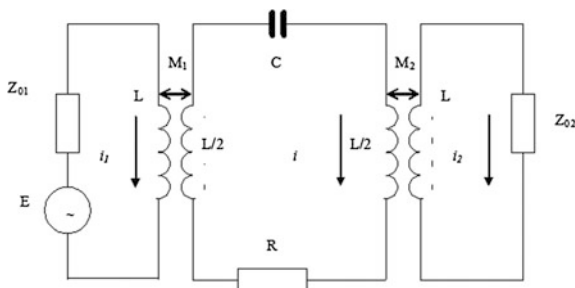


where: $\omega$ is angular frequency, $W$ is energy stored in the resonator for the period of oscillation, $P_T$ is power of heat loss; $P_c$ is power transferred in the transmission line by waves which reradiated by resonator.

The coupling coefficient of the resonator with microwave transmission line is defined as the ratio of the own quality factor to quality factor of coupling:

$$K = \frac{Q_0}{Q_c} \qquad (13)$$

For calculation of coefficients of reflection, transmission and absorption we obtain the energy relations for the system of two transmission lines connected by ME resonator. Transmission and reflection coefficients is defined as the ratio of the amplitudes fields considering only the basic wave type. The equation of power balance in the system at resonance is follows:

$$P_{in} = P_{in}T^2 + P_{in}R^2 + P_{in}A^2 \qquad (14)$$

where $T$ is transmission coefficient; $R$ is reflection coefficient; $A$ is absorption coefficient.

Relations for the transmission, reflection and absorption coefficients can be obtained by analysis of the equivalent circuit (Fig. 26). The resonator in the equivalent circuit is represented as $LCR$ oscillation circuit. Full input and output impedance of the transmission line can be calculated by analysis of the equivalent circuit first, and then it is possible to calculate the transmission and reflection coefficients, submitted through the coupling coefficient. This equivalent circuit can be applied to analysis of microstrip and waveguide resonant microwave power sensors.

Either all coefficients can be obtained by solving the equation of power balance. At the same coupling between the resonator and the input and output transmission lines, these formulas take the form:

$$T = \frac{K}{1+K}; R = \frac{1}{1+K}; A = \frac{2K}{(1+K)^2} \qquad (15)$$

The coupling coefficient is calculated as follows:

$$K = \frac{1 - R}{R} = \frac{|T|}{1 - |T|} \tag{16}$$

To use the obtained general relations in specific cases it is necessary to calculate the coupling coefficients of the resonator with the transmission line. Considerable practical interest present a combination of a ME resonator with microstrip transmission line, which leads to a number of wideband, compact and easy-to-manufacture devices. The coupling coefficient in this case can be represented as:

$$K = \frac{2V\chi''_+ z_0 \varepsilon}{\pi h^2 \lambda_v Z} \left( \text{arctg} \frac{Z}{z_0 \sqrt{\varepsilon}} + \frac{1}{3} \text{arctg} \frac{3Z}{z_0 \sqrt{\varepsilon}} \right)^2 \tag{17}$$

$$\chi''_+ = \frac{8\pi M_0}{\Delta H}$$

where: $M_0$ is the saturation magnetization of the ferrite component; $\Delta H$ is the half-width of the FMR line; $z_0$ is characteristic impedance of a microstrip transmission line; $V$ is volume of the ME resonator; $\chi''_+$ is a magnetic susceptibility at resonance; $Z$ is wave impedance of free space; $\varepsilon$ is the permittivity of the substrate, $h$ is the substrate thickness; $\lambda$ is wavelength transmission line.

Thus, using the expression for the coupling coefficient and the general formulas for the characteristics of the transmission line it can be calculated coefficients of reflection, transmission and absorption for different schemes of inclusion of ME resonators, and therefore devices.

The degree of coupling is characterized by the coefficient of transmission of microwave electromagnetic energy. Here we consider the transmission coefficient when the ME resonator is as heterogeneity in the transmission line.

If the transmission line is completely matched, power absorbed by ME resonator can be written as:

$$P_{ab} = \varkappa P_{in} \tag{18}$$

where the absorption coefficient is given by:

$$\varkappa = \frac{4K}{(1 + K)^2 + \xi^2} \tag{19}$$

where: $K$ is ME coupling coefficient of the resonator to the transmission line, is normalized detuning of magnetic field from the resonance values:

$$\xi = \frac{H_p - H_0 + \delta H_E}{\Delta H} \tag{20}$$

where: $Hp$ is the value of the resonance field for a given frequency; $H_0$ is constant magnetizing field; $\delta H_E$ is the value of resonance shift under the influence of applied electric field; $\Delta H$ is the half-width of the resonance curve of ME sample.

Absorption of microwave power by the ME material can be described by an effective magnetic microwave field $\boldsymbol{h}$ due to the ME interaction, while the absorbed power is equal to:

$$P_{ab} = k_l \boldsymbol{h}^2 \tag{21}$$

where $k_l$ is coefficient depending on the shape and properties of the sample and equal for the disk, magnetized perpendicular or spherical sample:

$$k_l = \frac{\pi M_0}{\Delta H} \mu_0 \omega V \tag{22}$$

for disk, magnetized tangential:

$$k_l = \frac{2\pi M_0}{\Delta H} - \frac{4\pi M_0 + H_0}{4\pi M_0 + 2H_0} \mu_0 \omega V \tag{23}$$

where $V$ is sample volume.

Magnetoelectric susceptibility tensor $\widehat{\chi}^{ME}$ is determined as:

$$\widehat{\chi}^{ME} = \widehat{\chi}^M \frac{h}{e} \tag{24}$$

where $\widehat{\chi}^M$ is magnetic susceptibility tensor

From the Formula (22) follows that electric field arising in ME element of microwave power sensor:

$$e = \frac{\widehat{\chi}^M \sqrt{\frac{4KP_{in}}{k_l\left[(1+K)^2 + \xi^2\right]}}}{\widehat{\chi}^{ME}} \tag{25}$$

The voltage on the ME element, which is a planar structure with electrodes (as capacitor) is:

$$U = ed = d \frac{\widehat{\chi}^M \sqrt{\frac{4KP_{in}}{k_l\left[(1+K)^2 + \xi^2\right]}}}{\widehat{\chi}^{ME}} \tag{26}$$

where: $d$ is the distance between the electrodes.

Sensitivity of microwave power sensor can be calculated by the formula:

$$K_U = d \frac{\widehat{\chi}^{ME} \sqrt{\frac{4K}{k_l\left[(1+K)^2 + \xi^2\right]}}}{\widehat{\chi}^M} \qquad (27)$$

Analysis of the formula (27) shows that for increasing the sensitivity of the microwave power sensor is necessary to use a material with a large ME suscepti-bility. Increasing the sensitivity will also decrease the magnetic susceptibility and the coupling coefficient. To obtain maximum sensitivity is necessary to provide adjustment of ME resonator on the resonant frequency.

## 5.3 Fabrication

### 5.3.1 Microstrip Resonant Microwave Power Sensor

The topology of the microstrip resonant microwave power sensor [54] is shown in Fig. 27.

ME material (5) is placed in the hole in the substrate (8), while its thickness must be equal to the thickness of the substrate. At the location of the ME material stripe loops (3) and (4) long $3\lambda/8$ and $\lambda/8$, respectively established area of circular polarization of the microwave field. ME material at the same time is in the field of a
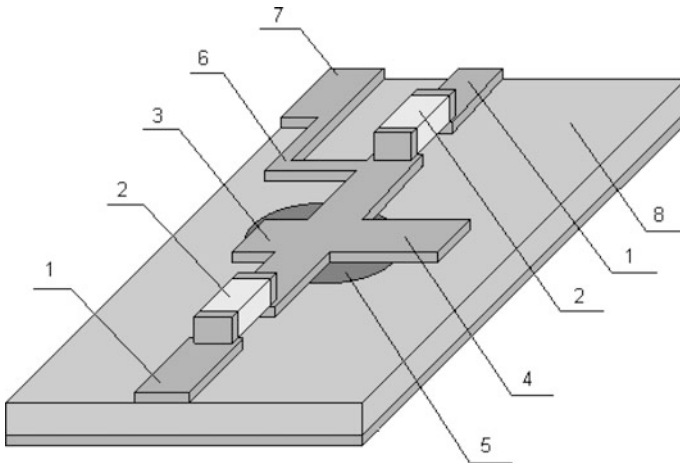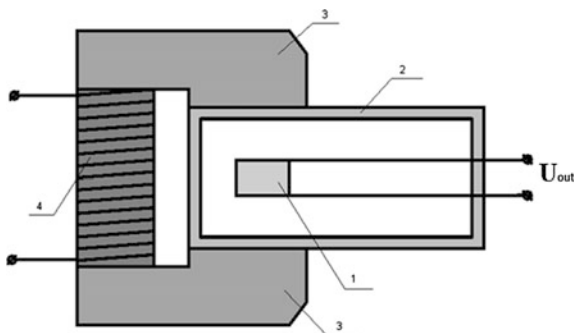


**Fig. 27** The topology of the microstrip microwave power sensor. (*1*) Is supply lines; (*2*) the coupling capacitor; (*3*, *4*) strip resonator; (*5*) ME material; (*6*) the inductive element; (*7*) the capacitive element; (*8*) substrate

**Fig. 28** ME waveguide microwave power sensor. (*1*) Is ME element; (*2*) the waveguide; (*3*) electromagnet poles; (*4*) the electromagnet coil

permanent magnet that produces magnetic bias field. The value of the magnetizing field determines the operating frequency of the sensor. On the electrodes of ME resonator due to passing through the sensor microwave power as a result of the ME interaction will appear ac voltage proportional to the incident power. The ac voltage, in the form of repeating the bending around amplitude-modulated RF signal through a low-pass filter (6 and 7) is connected to a measuring device. Coupling capacitors (2), without affecting the microwave signal, prevent the spread of low-frequency voltage across the RF channel.

Presented power sensor can be used as a detector of amplitude-modulated microwave oscillations.

### 5.3.2 Waveguide Resonance Microwave Power Sensor

Microwave power sensor (Fig. 28) is a waveguide device. ME element is placed in the area of circular polarization, while being in a constant magnetic field of electromagnet which create magnetic bias field at resonance frequency. The value of the magnetizing field will determine the operating frequency of the sensor. On the electrodes of ME material will appear ac voltage repeating form of the bending around of the microwave signal and proportional to the measured power.

Presented sensor operates at a frequency determined by the voltage of resonant constant magnetic field. The frequency rearrange of the waveguide microwave power sensor is achieved by varying the value of the magnetizing field. The waveguide sensor can be used as a detector of an amplitude-modulated microwave oscillations.

### 5.3.3 ME Microwave Power Sensor Based on Toroidal Resonator

Figure 29 shows the design of the sensor on the basis of the toroidal resonator [55]. ME element (1) is placed at an antinodes of the ac electric field and simultaneously in the field of the permanent magnet (3). Coil (5) based on thin-film technology are

Fig. 29 ME microwave
power sensor based on a
toroidal resonator. (*1*) Is ME
element; (*2*) the toroidal
resonator; (*3*) the permanent
magnet; (*4*) electromagnet
poles. (*5*) coil
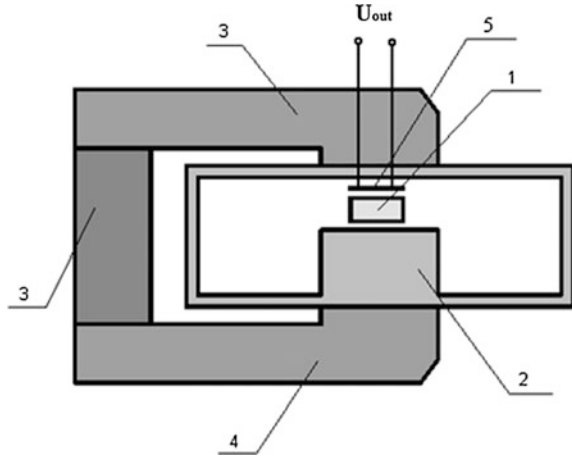
placed directly on the surface of the resonator ME. The value of resonance magnetizing field will determine the operating frequency of the sensor.

Under the action of the ac electric field on ME resonator through the piezoelectric and magnetostrictive action around the ME resonator will appear low-frequency ac magnetic field. Due to inductive coupling of ME resonator and the coil on the electrodes arise EMF in the shape corresponding to the bending around of the amplitude-modulated microwave signal, and the amplitude is proportional to the measured power. Presented sensor operates at a fixed frequency determined by the voltage of the constant magnetic field and the self-resonant frequency of the toroidal resonator. When using an electromagnet, and a mechanical adjustment of the toroidal resonator it can be changed the operating frequency of the sensor.

The main advantage of ME microwave power sensor on the basis of the toroidal resonator is: (1) the ability to measure high power levels at which the traditional ferrite sensors and ME sensors operating in an ac microwave field are in the saturation regime; (2) ac microwave electric and magnetic fields sufficiently separated and haven't influence simultaneously at large ME resonators.

# 6 Conclusions

In this chapter we considered the main constructions, equivalent circuits and characteristics of ME sensors for measuring the magnetic field, current in conductor and microwave power. It was showed that ME sensors have some advantages over semiconductor ones, for example based on Hall effect, in the sensitivity, low price and radiation resistance.

Obtained results are as follows:

(1) The nomograph method is suggested for the efficient estimates of ME voltage coefficients from given parameters of composite components. This facilitates to evaluate the feasibility of the composite for sensor application.

(2) The potential for ME sensors is notable due to the fact that there are no other present generations of magnetic sensors having the following key requirements: extreme sensitivity ($\sim pT/Hz^{1/2}$), allowing for better magnetic anomaly detection; zero power consumption to foster long-term operation; operation at low frequencies, $f \sim 1$ Hz; miniaturize size, enabling deployment of arrays; and low cost.

(3) The theory predicts that the highly sensitive ME laminate can be designed by increasing the ME voltage coefficient.

(4) ME sensitivity optimization should take into account the environmental or external noise sources, such as thermal fluctuation and mechanical vibration. These external noises will be dominating factors that affect the sensor's sensitivity in practical applications. For ME sensors, the dominant ones are the thermal fluctuation and mechanical vibration sources. It is important that ME sensors are designed by such a means that optimizes its abilities to cancel these external noise.

(5) The output voltage of ME current sensor was found to be a function of the detecting input current under various dc magnetic bias fields. The sensor sensitivity depends on constructive and material parameters of ME composite and bias magnetic field. The operating point for the ME current sensor has been selected. Current sensing based on ME effect is a good choice for many applications due to galvanic isolation between the sensed circuit and the measuring circuit. Using push-pull mode of ME composite will enable an improvement of the sensors. For increasing the sensor sensitivity one needs to use the ME composite based on materials with high magnetostriction and piezoelectric coupling.

(6) Analysis of characteristics of the microwave power sensors shows that one of the most promising ways to improve the sensors is the use of ME materials, which allows improving the performance of devices, expand their functionality and, in some cases, to create sensors with properties which are unobtainable in other microwave power sensors. Sensors based on composite materials have a wide frequency range up to hundreds of gigahertz, stable to significant levels of radiation, temperature range is from 0 K to the Curie temperature. In the microwave range, it is possible to use selective properties of ME materials, that allows to create a frequency selective power sensor with the possibility of adjustment.

Future prospects:

Although a large number of parameters of ME sensors would be attained, however, several important issues remain to be solved, including, the following.

(1) Increasing the sensitivity and design of sensor for simultaneous measuring the orientation and magnitude of dc and ac magnetic field.

(2) Design of contactless sensor and one for measuring the current at different range from leakage current up to 100 A.

(3) Realization of frequency tuning and design of sensor at different range of microwave power.

# References

1. M.I. Bichurin, D. Viehland (eds.) *Magnetoelectricity in Composites* (Pan Stanford Publishing, Singapore, 2012), 273 p

2. C.-W. Nan, M.I. Bichurin, S. Dong, D. Viehland, G. Srinivasan, J. Appl. Phys. **103**, 031101 (2008)

3. B.D.H. Tellegen, Philips Res. Rep. **3**, 81 (1948)

4. J.Y. Zhai, J.F. Li, S.X. Dong, D. Viehland, M.I. Bichurin, J. Appl. Phys. **100**, 124509 (2006)

5. M.I. Bichurin, V.M. Petrov, R.V. Petrov, Y.V. Kiliba, F.I. Bukashev, A.Y. Smirnov, D.N. Eliseev, Ferroelectrics **280**, 199 (2002)

6. Y. Wang, J. Li, D. Viehland, Mater. Today **17**, 269 (2014)

7. H. Schmid, Ferroelectrics **162**, 317 (1994)

8. J. Van Suchtelen, Philips Res. Rep. **27**, 28 (1972)

9. J. van den Boomgaard, A.M.J.G. van Run, J. van Suchtelen, Ferroelectrics **14**, 727 (1976)

10. M.I. Bichurin, D. Viehland, G. Srinivasan, J. Electroceram. **19**, 243–250 (2007)

11. D.N. Astrov, Sov. Phys. JETP **13**, 729 (1961)

12. S. Dong, J. Zhai, F. Bai, J.F. Li, D. Viehland, Appl. Phys. Lett. **87**, 062502 (2005)

13. C.-W. Nan, G. Liu, Y. Lin, H. Chen, Phys. Rev. Lett. **94**, 197203 (2005)

14. S. Dong, J. Zhai, J. Li, D. Viehland, Appl. Phys. Lett. **89**, 252904 (2006)

15. M.I. Bichurin, V.M. Petrov, S. Priya, Magnetoelectric Multiferroic Composites (Chap. 12), in *Ferroelectrics—Physical Effects*, ed. by M. Lallart (InTech, 2011), p. 277

16. J. Zhai, Z. Xing, S. Dong, J. Li, D. Viehland, J. Am. Ceram. Sos. **91**, 351 (2008)

17. G. Harshe G, Magnetoelectric effect in piezoelectric-magnetostrictive composites. PhD thesis, The Pennsylvania State University, College Park, PA, 1991

18. M.I. Bichurin, V.M. Petrov, in *Modeling of Magnetoelectric Effects in Composites*, vol. 201. Springer Series in Materials Science (Springer, New York, 2014), 108p

19. M.I. Bichurin, V.M. Petrov, R.V. Petrov, Y.V. Kiliba, F.I. Bukashev, A.Y. Smirnov, D.N. Eliseev, Ferroelectrics **280**, 365 (2002)

20. J. Gao, Y. Wang, M. Li, Y. Shen, J. Li, D. Viehland, Mater. Lett. **85**, 84–87 (2012)

21. J. Clarke, R.H. Koch, The impact of high-temperature superconductivity on SQUID magnetometers. Science **242**, 217–223 (1988)

22. Y.J. Wang, J.Q. Gao, M.H. Li, Y. Shen, D. Hasanyan, J.F. Li, D. Viehland, Phil. Trans. R. Soc. A **372**, 20120455 (2014)

23. Y. Wang, D. Gray, J. Gao, D. Berry, M. Li, J. Li, D. Viehland, H. Luo, J. Alloy. Compd. **519**, 1–3 (2012)

24. Y. Wang, D. Gray, D. Berry, J. Li, D. Viehland, IEEE Trans. Ultrason. Ferroelectr. Freq. Control **59**, 859–862 (2012)

25. Y. Wang, J. Gao, M. Li, D. Hasanyan, Y. Shen, J. Li, D. Viehland, H. Luo, Appl. Phys. Lett. **101**, 022903 (2012)

26. X. Zhuang, S. Saez, M. Lam Chok Sing, C. Cordier, C. Dolabdjian, J. Li, D. Viehland, S.K. Mandal, G Sreenivasulu, G. Srinivasan, Sens. Lett. **10**, 961 (2012)

27. R. Jahns, H. Greve, E. Woltermann, E. Quandt, R. Knöchel, Sens. Actuators, A **183**, 16 (2012)

28. T. Onuta, Y. Wang, S.E. Lofland, I. Takeuchi, Adv. Mater. (2014). doi:10.1002/adma.201402974
29. S. Marauska, R. Jahns, C. Kirchhof, M. Claus, E. Quandt, R. Knochel, B. Wagner, Sens. Actuators, A **189**, 321 (2013)
30. J. Petrie, D. Viehland, D. Gray, S. Mandal, G. Sreenivasulu, G. Srinivasan, A.S. Edelstein, J. Appl. Phys. **111**, 07C714 (2012)
31. J.R. Petrie, J. Fine, S. Mandal, G. Sreenivasulu, G. Srinivasan, A.S. Edelstein, Appl. Phys. Lett. **99**, 043504 (2011)
32. Y. Wang, D. Gray, D. Berry, J. Gao, M. Li, J. Li, D. Viehland, Adv. Mater. **23**, 4111 (2013)
33. E. Lage, C. Kirchhof, V. Hrkac, L. Kienle, R. Jahns, R. Knöchel, E. Quandt, D. Meyners, Nat. Mater. **11**, 523 (2012)
34. C. Kirchhof, M. Krantz, I. Teliban et al., Appl. Phys. Lett. **102**, 232905 (2013)
35. A. Piorra, R. Jahns, I. Teliban et al., Appl. Phys. Lett. **103**, 032902 (2013)
36. G. Sreenivasulu, V.M. Petrov, L.Y. Fetisov, Y.K. Fetisov, G. Srinivasan, Phys. Rev. B **86**, 214405 (2012)
37. T.T. Nguyen, F. Bouillault, L. Daniel, X. Mininger, Finite element modeling of magnetic field sensors based on nonlinear magnetoelectric effect. J. Appl. Phys. **109**, 084904 (2011)
38. M.I. Bichurin, V.M. Petrov, R.V. Petrov, Y.V. Kiliba, F.I. Bukashev, A.Y. Smirnov, D.N. Eliseev, Ferroelectrics **280**, 365 (2002)
39. S.X. Dong, J.F. Li, D. Viehland, J. Appl. Phys. **96**, 3382 (2004)
40. S.X. Dong, J.F. Li, D. Viehland, Appl. Phys. Lett. **85**, 2307 (2004)
41. Shuxiang Dong, John G. Bai, Junyi Zhai et al., Appl. Phys. Lett. **86**, 182506 (2005)
42. S. Zhang, C.M. Leung, W. Kuang, S.W. Or, S.L. Ho. J. Appl. Phys. **113**, 17C733 (2013)
43. S.X. Dong, J.G. Bai, J.Y. Zhai, J.F. Li, G.Q. Lu, D. Viehland, S.J. Zhang, T.R. Shrout, Appl. Phys. Lett. **86**, 182506 (2005)
44. Jitao Zhang, Ping Li, Yumei Wen, Wei He et al., Rev. Sci. Instrum. **83**, 115001 (2012)
45. R.V. Petrov, N.V. Yegerev, M.I. Bichurin, S.R. Aleksić, Current sensor based on magnetoelectric effect, in *Proceedings of XVIII-th International Symposium on Electrical Apparatus and Technologies SIELA 2014*, , Bourgas, Bulgaria, 29–31 May 2014
46. I.N. Solovyev, A.N. Solovyev, R.V. Petrov, M.I. Bichurin, A.N. Vučković, N.B. Raičević. Sensitivity of magnetoelectric current sensor, in *Proceedings of 11th International Conference on Applied Electromagnetics—ПЕС 2013*, Niš, Serbia, 1–4 Sept 2013, pp. 109–110
47. R.V. Petrov, I.N. Solovyev, A.N. Soloviev, M.I. Bichurin, Magnetoelectic current sensor, in *PIERS Proceedings*, Stockholm, Sweden, 12–15 Aug 2013, pp. 105–108
48. M. I. Bichurin, V.M. Petrov, Modeling of magnetoelectric interaction in magnetostrictive-piezoelectric composites, in *Advances in Condensed Matter Physics* (2012)
49. E.L. Ginzton, *Microwave Measurements* (McGraw-Hill, Inc., London, 1957)
50. A. Fantom, *Radio Frequency and Microwave Power Measurement*, IET (1990), 278p
51. M.I. Bichurin, S.V. Averkin, G.A. Semenov, The magnetoelectric resonator. Patent 2450427RU
52. A.S. Tatarenko, M.I. Bichurin, Electrically tunable resonator for microwave applications based on hexaferrite-piezoelectrc layered structure. Am. J. Condens. Matter Phys. **2**, #5 (2012)
53. M.I. Bichurin, V.M. Petrov, G.A. Semenov, Magnetoelectric material for components of radio-electronic devices. Patent 2363074RU
54. M.I. Bichurin, S.N. Ivanov, Selective microwave power detector. Patent 2451942RU
55. M.I. Bichurin, A.S. Tatarenko, V. Kiliba Yu, Magnetoelectric microwave power sensor. Patent 147272RU